the control vector pCXL or pCXLB, harboring the *attB* sequence with or without a ϕC31 integrase-expression vector, pCMVInt. Using a previously established method for determining integration efficiency [13], we measured the luciferase activity through several passages. In comparison with the extinction observed with the other combinations, the stability of luciferase expression in the presence of both integrase and *attB* was modest but reproducibly higher for 12 days (Figure 1B). We therefore confirmed that the ϕC31 integrase system can promote integration in T-cell lines.

Next, we wished to determine whether the ϕC31 integrase/*attB* system would mediate site-specific integration in hematopoietic cells. First, we established T-cell clones and examined the integration sites. We used the Jurkat T-cell line, since the experiments described above indicated that stable transfectants could be established with this cell line, enabling further investigation of the integration sites over the long term. Jurkat cells were transfected with equal amounts of pCMVInt and pcDNA-attB; the latter contained both the *attB* sequence and the *neo*^{r} gene. After the G418 selection, stable clones were obtained and subjected to integration site analysis. To determine the genomic locations of the integration sites, we applied the LAM-PCR method with genomic DNA prepared from each clone. Since we used G418-resistant clones, a specific single band was obtained (Figure 2A). The *attB* flanking sequences were further analyzed and the chromosomal loci were identified. By using the tumor gene database, we determined that among the 30 integration sites sequenced, no integrations were in or close to the LMO-2 or other known proto-oncogene loci (Table 1). Although several tumor-related genes exist at the same general loci as the ones identified as integration sites in this study, in all cases, their transcription initiation sites were far from the integrated vectors (in terms of at least the surrounding 100 kb), suggesting that there should be little if any effect on their transcriptional activation. This finding is important, because there is a strong relationship between combinatorial insertion events and serious adverse effects [25–27].

Since a primary objective was to determine the site-specificity of the ϕC31 integrase in hematopoietic cells, we next investigated the previously known pseudo-*attP* sequences in identified loci. Interestingly, among the 30 clones, we did not detect any integration events at the previously reported hpsA human pseudo-*attP* site on chromosome 8p22, a well-characterized ϕC31-mediated integration site in the human genome, which has been studied in various cell lines and tissues, including 293 cells, myoblasts, and keratinocytes [13,17,18]. To verify the insignificant level of insertion into the hpsA, we tested another genomic PCR fragment using a different PCR primer pair to amplify the hpsA-vector 'junction' site, and again detected no insertion into the site (data not shown). These results suggested that the hpsA was not frequently used in T cells. Instead, among the Jurkat clones, we identified two closely related integration sites that were each used three times in this set of 30 clones. The independence of the integration events was

Table 1. Integration sites recovered by LAM-PCR from clones derived from Jurkat cells cultured for 3 weeks. Integration loci were identified using the National Center for Biotechnology (NCBI) BLAST search and MAP viewer. Tumor genes were defined using the tumor gene database. Notably, a total of three clones were each integrated at chromosomes 13q14.1 and 18p11.2. TSS stands for 'transcription start site'

Locus	Tumor genes on the locus	Position to TSS (kb)	Other genes on the locus	Number of clones
1q31	–	–	PTPRC,LOC391147	1
1q42.3	–	–	TBCE,GGPS1	1
2q11.2	–	–	CNGA3,INPP4A	1
3p23	–	–	SATB1,LOC401056	1
5q13.3	–	–	F2R,F2RL1	1
5q14	–	–	COX7C,LOC389308	1
6p21.3	–	–	CYCSL1,GRM4	1
7q21.2	–	–	RN7SLP4,LOC442597	1
7q36	–	–	hIAN7,HIMAP4	1
8q13	–	–	NCOA2,TRAM1	1
8q24.1	MYC	>100	LOC401476	1
10q22.1	–	–	PCBD,UCN5B	1
10q25	–	–	SHOC2,ADRA2A	1
13q12.2	BRCA1, FLT1	>100	ZMYM5,LOC400099	1
13q14.1	RB1, TSC-22	>100	WBP4,KBTBD6	3
13q31	–	–	LOC150928	1
13q33	–	–	FLJ40176,LOC196541	1
15q25	fur	>100	FLJ12587	1
16q24	–	–	KIAA0182	1
17q12	–	–	SNIP,ARHGAP23	1
17q25	–	–	ITGB4,GALK1	1
18p11.2	–	–	TNFSF5IP1,C18orf9	3
18q22	–	–	ZNF236,MBP	1
19q13.2	BCL3, AKT2	>100	ZNF223,KCNN4	1
21q22.2	–	–	C21orf18,C21orf96	1
Xq22.1	–	–	DRP2,TAF7L	1

A

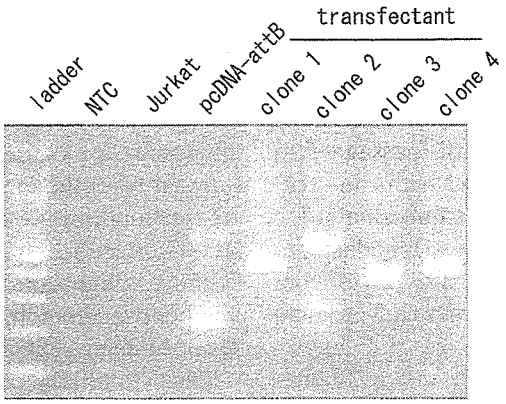

B

```
B' arm                                          GGCTCCCCGGGCGCGTACTCCACC
  JD9   gcagctgcaatcggagtcaccacttggttaagcttGGCTCCCCGGGCGCGTACTCCACC
  JD21  gcagctgcaatcggagtcaccacttggttaagct:GGCTCCCCGGGCGCGTACTCCACC
  JD11  gcagctgcaatcggagtcaccacttgg::::::::GGCTCCCCGGGCGCGTACTCCACC
```

C

Site	Sequence	% identity to attP
WT attP	CCCCAACTGGGGTAACCTT-TGAGTTCTCTCAGTTGGGGG	100%
13q14.1	TCACCACTTGGTTAAGCTTATGATAATCCACCGTGATTCT	51%
18p11.2	TCACCACTTGGTTAAGCTTAAGATAATCCACTGTCATTCT	49%

D

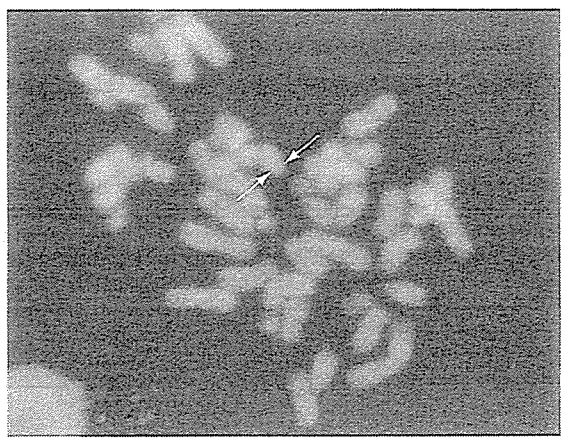

Figure 2. (A) LAM-PCR analysis of clones derived from Jurkat cells. The products of the final exponential PCR are shown. Genomic DNA from parental Jurkat cells was used as a negative control, and the exogenous plasmid pcDNA-attB was used as a positive control. NTC stands for 'no template control'. A specific PCR amplification was obtained from each clone. (B) The sequence of the crossover region between the 13q14.1 pseudo-site and the ϕC31 *attB* site. The small deletion observed ranged from one to eight nucleotides. ϕC31 pseudo-*attP* sequences. (C) Two ϕC31 pseudo-*attP* sequences are compared with the wild-type *attP* sequence. Thirty-nine base pairs of each *attP* sequence are shown. The pseudo-*attP* sites are named for their chromosomal positions at 13q14.1 and 18p11.2. Wild-type *attP* and the 13q14.1 pseudo-site have 51% similarity, if a 1-bp gap is inserted in the middle of the wild-type *attP* core. The 18p11.2 sequence shows striking similarity, although it differs in the three nucleotides shown in red. (D) FISH analysis of clone JD1 harboring the *attB* donor vector, showing hybridization at 18p11.2. Two identical green vector-specific signals were detected at 18p11.2 (arrow); the chromosomes were visualized by DAPI (blue)

confirmed by the slightly different sequences observed within crossover junctions (Figure 2B). BLAST analysis of one of the integration sites revealed that it was located on chromosome 13p14.1, in an intergenic ERVL repeat element. ERVL repeats represent sequences of defective endogenous retroviruses and are dispersed throughout the genome [28]. Sequence alignment between wild-type *attP* and the chromosome 13p14.1 integration site revealed significant similarity, amounting to 51% if a 1-bp gap was inserted into the wild-type *attP* site near the core, confirming the likelihood of it being a ϕC31 pseudo-*attP* site (Figure 2C). This integration site was also seen repeatedly in a study analyzing ~200 integration events in three non-hematopoietic human cell lines [29]. Therefore, the 13p14.1 site seems to be a preferred integration site in many cell

types. Several of the other integration sites listed in Table 1, such as 19q13 and Xq22.1, were also found to be common pseudo-sites in other human cell lines [29].

In addition to the three clones integrated at chromosome 13p14.1, we also found three integration events whose DNA sequences placed them in an ERVL element on chromosome 18p11.2. This novel pseudo-*attP* site is very similar in sequence to the one on chromosome 13p14.1, as illustrated in Figure 2C. A Jurkat clone JD1 shown by LAM-PCR analysis to harbor the *attB* plasmid at the chromosome 18p11.2 site was then subjected to FISH analysis. The signals were found at the 18p11.2 locus as predicted by the BLAST search, further confirming the validity of the LAM-PCR method (Figure 2D). We further examined the integration at the 18p11.2 pseudo-site in two of the clones, JD1 and JD16, by genomic PCR. Although one of the primers was designed to match the distal part of the genome from the *attP* homology region, similarly sized PCR products were obtained for both clones, again confirming our LAM-PCR results (Figure 3A).

Next, to address the feasibility of SCID-X1 gene therapy mediated by the ϕC31 integrase, we tested genomic integration into a human T-cell line, ED40515(-), that is defective in the expression of γc [21]. For this purpose, a γc-expression plasmid bearing an *attB* sequence, pCXγB, was newly constructed (Figure 1A). We transfected the ED40515(-) cells with the therapeutic plasmid pCXγB, along with the pCMVInt ϕC31 integrase expression vector, by electroporation. After selection for G418 resistance, stably transfected clones were obtained. To determine whether ϕC31-mediated integration of pCXγB into the newly identified pseudo-*attP* sites had occurred, a genomic PCR amplification was carried out. Among the 24 clones analyzed, we failed to identify any integration events at the 13q14.1 pseudo-*attP* site, but one clone (4.2%), designated as EDγi6, gave PCR amplification corresponding to the 18p11.2 pseudo-site (Figure 3A). Since the 18p11.2 pseudo-site was an active ϕC31 integration site not only in Jurkat but also in ED40515(-) cells, we believe that this site may be a preferred target for ϕC31 integrase-mediated therapeutic gene delivery in hematopoietic cells.

To assess the validity of the integrase system as an alternative SCID-X1 gene therapy strategy, we examined whether integration of the γc-expression vector into the chromosome 18p11.2 site produced a functional γc protein. Flow cytometric analysis revealed robust γc expression (Figure 3B). Because the analysis was performed after 3 months of culture and at least 25 passages, ϕC31-mediated integration of the therapeutic gene was stable in terms of long-term integration, expression, and function. Finally, we examined the correction of IL-2-mediated signal transduction by monitoring the tyrosine-phosphorylation status of STAT5. A functional IL-2 receptor complex delivers signals by activating the JAK1 and JAK3 kinases, which further phosphorylate and activate the transcription factor

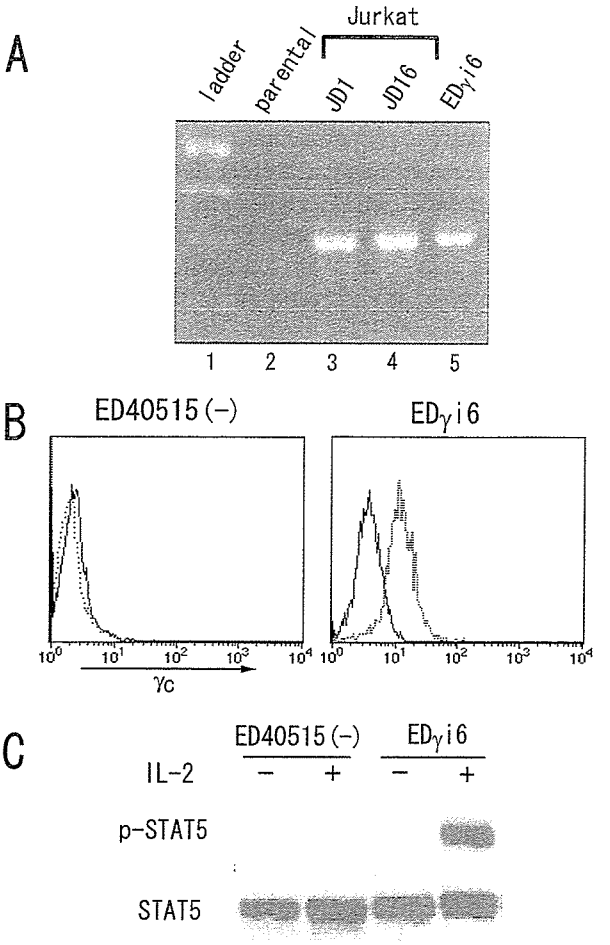

Figure 3. (A) Detection of integrase-mediated site-specific integration at 18p11.2. Genomic DNA purified from parental ED40515(-) cells was used as a control (lane 2). EDγi6, an established clone generated by the electroporation of equal amounts of pCMVInt and pCXγB (lane 5), gave appropriate PCR amplification bands of a size comparable to those seen in the two established clones derived from Jurkat cells (lanes 3 and 4). (B) Flow cytometric analysis of the γc expression of parental ED40515(-) and EDγi6 cells. Cells were labeled either by the anti-human γc mAb (dashed lines) or its isotype control antibody (solid lines). (C) ED40515(-) and EDγi6 cells were stimulated with IL-2. Western blot analysis was performed with the indicated antibodies. IL-2-induced tyrosine phosphorylation of STAT5 was observed in EDγi6

STAT5. Following stimulation with IL-2, EDγi6, but not the parent ED40515(-) cells, showed significant phosphorylation of STAT5 (Figure 3C). We therefore concluded that ϕC31 integrase-mediated gene delivery into hematopoietic cells may be a potential alternative therapeutic technology for SCID-X1, as judged by its site-specific integration and successful reconstitution of functional IL-2 receptor complexes.

Discussion

In the present study, we demonstrated that the phage ϕC31 integrase introduced plasmids containing the *attB* sequence into endogenous sites in the chromosomes of

human T-cell lines. We speculate that ERVL repeats on chromosomes 13 and 18 may represent frequent integration sites in hematopoietic cells. The ERVL repeats have slight sequence differences between them and lie in different chromosomal contexts [28], which may help determine why different ERVL repeats are used as preferential ϕC31 integration sites in different tissues. Because the dysregulation of γc expression may contribute to oncogenesis, in future studies it may be preferable to place the γc gene under the control of its own native promoter [30], rather than that of a widely expressed constitutive promoter.

Although some integrated transgenes are reportedly prone to decrease their transcription activity, probably due to epigenetic modifications such as DNA methylation [31], our observation that the γc transgene retained activity for at least 3 months suggests a potential advantage of the ϕC31 integrase technology for modifying hematopoietic cells. Previous studies have documented that the ϕC31 integrase facilitates genomic integration. For example, in 293 cells, the isolation of stable colonies increased at least five-fold when the ϕC31 integrase gene was co-transfected [13]. Under our experimental conditions with Jurkat cells, the increase was more modest, around two- to three-fold. At present, the reason for the less-efficient integration in Jurkat cells than in other cell lines including 293 is unclear. In general, to improve the effectiveness of this technology, two key achievements are needed: (1) the DNA transfection efficiency into the target cells should be increased, and (2) the DNA integration efficiency in the transfected cells should be increased. Since our present ϕC31 integrase system has at least succeeded in increasing the integration efficiency, we next need to develop an efficient transfection methodology for HSCs. One intriguing possibility may be to combine the high transduction efficiency of a virus vector with the ϕC31 integrase [32,33]. Further studies will be needed to increase the integration efficiency by using alternative transduction technologies and/or by manipulating the integrase itself [34].

For future application of this methodology to SCID-X1 treatment using HSCs, it will be important to avoid unfavorable integration sites that could trans-activate proto-oncogenes [26,27,35]. While we found no obvious integration sites in or close to known proto-oncogenes that could potentially be activated in *cis* by a promoter insertion mechanism, other integration sites not revealed in this study may pose a risk. A more comprehensive study of the integration specificity of ϕC31 integrase in human cell lines revealed ~100 integration sites and a prediction of a total of ~370 potential integration sites [29]. While analysis of the known integration sites against a database of cancer genes including both oncogenes and tumor suppressor genes revealed no alarming associations, *in vivo* transformation assays would be helpful in assessing cancer risk of the ϕC31 system. The existing frequent integration at the two intergenic ERVL sites suggests that directed evolution of the integrase toward an increased preference for this or other safe integration sites may further reduce the risk of insertional mutagenesis [36]. Our current study suggests the possibility of utilizing ϕC31 integrase-mediated gene delivery as a promising approach for future SCID-X1 gene therapies.

Acknowledgements

The authors thank Dr. Lishomwa Ndhlovu for critically reading the manuscript. This work was supported in part by the 21st Century Center of Excellence (COE) Program, a Grant-in-Aid for Scientific Research from the Japan Society for the Promotion of Science, a Grant-in-Aid for Scientific Research on Priority Areas from the Ministry of Education, Science, Sports, and Culture, a Grant-in-Aid from the Ministry of Health, Labor, and Welfare of the Japanese Government, and NIH grant HL68112 to M.P.C.

References

1. Sugamura K, Asao H, Kondo M, *et al.* The interleukin-2 receptor gamma chain: its role in the multiple cytokine receptor complexes and T cell development in XSCID. *Annu Rev Immunol* 1996; **14**: 179–205.
2. Buckley RH. Molecular defects in human severe combined immunodeficiency and approaches to immune reconstitution. *Annu Rev Immunol* 2004; **22**: 625–655.
3. Otsu M, Sugamura K, Candotti F. In vivo competitive studies between normal and common gamma chain-defective bone marrow cells: implications for gene therapy. *Hum Gene Ther* 2000; **11**: 2051–2056.
4. Fischer A, Hacein-Bey S, Cavazzana-Calvo M. Gene therapy of severe combined immunodeficiencies. *Nat Rev Immunol* 2002; **2**: 615–621.
5. Cavazzana-Calvo M, Hacein-Bey S, de Saint Basile G, *et al.* Gene therapy of human severe combined immunodeficiency (SCID)-X1 disease. *Science* 2000; **288**: 669–672.
6. Hacein-Bey-Abina S, Le Deist F, Carlier F, *et al.* Sustained correction of X-linked severe combined immunodeficiency by ex vivo gene therapy. *N Engl J Med* 2002; **346**: 1185–1193.
7. Gaspar HB, Parsley KL, Howe S, *et al.* Gene therapy of X-linked severe combined immunodeficiency by use of a pseudotyped gammaretroviral vector. *Lancet* 2004; **364**: 2181–2187.
8. Hacein-Bey-Abina S, Von Kalle C, Schmidt M, *et al.* LMO2-associated clonal T cell proliferation in two patients after gene therapy for SCID-X1. *Science* 2003; **302**: 415–419.
9. Couzin J, Kaiser J. Gene therapy. As Gelsinger case ends, gene therapy suffers another blow. *Science* 2005; **307**: 1028.
10. Kohn DB, Sadelain M, Glorioso JC. Occurrence of leukaemia following gene therapy of X-linked SCID. *Nat Rev Cancer* 2003; **3**: 477–488.
11. Baum C, von Kalle C, Staal FJ, *et al.* Chance or necessity? Insertional mutagenesis in gene therapy and its consequences. *Mol Ther* 2004; **9**: 5–13.
12. Groth AC, Calos MP. Phage integrases: biology and applications. *J Mol Biol* 2004; **335**: 667–678.
13. Thyagarajan B, Olivares EC, Hollis RP, *et al.* Site-specific genomic integration in mammalian cells mediated by phage phiC31 integrase. *Mol Cell Biol* 2001; **21**: 3926–3934.
14. Ginsburg DS, Calos MP. Site-specific integration with phiC31 integrase for prolonged expression of therapeutic genes. *Adv Genet* 2005; **54**: 179–187.
15. Olivares EC, Hollis RP, Chalberg TW, *et al.* Site-specific genomic integration produces therapeutic Factor IX levels in mice. *Nat Biotechnol* 2002; **20**: 1124–1128.
16. Held PK, Olivares EC, Aguilar CP, *et al.* In vivo correction of murine hereditary tyrosinemia type I by phiC31 integrase-mediated gene delivery. *Mol Ther* 2005; **11**: 399–408.
17. Ortiz-Urda S, Thyagarajan B, Keene DR, *et al.* Stable nonviral genetic correction of inherited human skin disease. *Nat Med* 2002; **8**: 1166–1170.

18. Quenneville SP, Chapdelaine P, Rousseau J, *et al.* Nucleofection of muscle-derived stem cells and myoblasts with phiC31 integrase: stable expression of a full-length-dystrophin fusion gene by human myoblasts. *Mol Ther* 2004; **10**: 679–687.
19. Niwa H, Yamamura K, Miyazaki J. Efficient selection for high-expression transfectants with a novel eukaryotic vector. *Gene* 1991; **108**: 193–199.
20. Asao H, Tanaka N, Ishii N, *et al.* Interleukin 2-induced activation of JAK3: possible involvement in signal transduction for c-myc induction and cell proliferation. *FEBS Lett* 1994; **351**: 201–206.
21. Maeda M, Shimizu A, Ikuta K, *et al.* Origin of human T-lymphotrophic virus I-positive T cell lines in adult T cell leukemia. Analysis of T cell receptor gene rearrangement. *J Exp Med* 1985; **162**: 2169–2174.
22. Schmidt M, Zickler P, Hoffmann G, *et al.* Polyclonal long-term repopulating stem cell clones in a primate model. *Blood* 2002; **100**: 2737–2743.
23. Niemitz EL, DeBaun MR, Fallon J, *et al.* Microdeletion of LIT1 in familial Beckwith-Wiedemann syndrome. *Am J Hum Genet* 2004; **75**: 844–849.
24. Kobayashi H, Tanaka N, Asao H, *et al.* Hrs, a mammalian master molecule in vesicular transport and protein sorting, suppresses the degradation of ESCRT proteins signal transducing adaptor molecule 1 and 2. *J Biol Chem* 2005; **280**: 10 468–10 477.
25. Dave UP, Jenkins NA, Copeland NG. Gene therapy insertional mutagenesis insights. *Science* 2004; **303**: 333.
26. Kustikova O, Fehse B, Modlich U, *et al.* Clonal dominance of hematopoietic stem cells triggered by retroviral gene marking. *Science* 2005; **308**: 1171–1174.
27. Modlich U, Kustikova OS, Schmidt M, *et al.* Leukemias following retroviral transfer of multidrug resistance 1 (MDR1) are driven by combinatorial insertional mutagenesis. *Blood* 2005; **105**: 4235–4246.
28. Lander ES, Linton LM, Birren B, *et al.* Initial sequencing and analysis of the human genome. *Nature* 2001; **409**: 860–921.
29. Chalberg TW, Portlock JL, Olivares EC, *et al.* Integration specificity of phage ϕC31 integrase in the human genome. *J Mol Biol* 2006; doi:10.1016/j.jmb.2005.11.098.
30. Ohbo K, Takasawa N, Ishii N, *et al.* Functional analysis of the human interleukin 2 receptor gamma chain gene promoter. *J Biol Chem* 1995; **270**: 7479–7486.
31. Klug CA, Cheshier S, Weissman IL. Inactivation of a GFP retrovirus occurs at multiple levels in long-term repopulating stem cells and their differentiated progeny. *Blood* 2000; **96**: 894–901.
32. Kubo S, Mitani K. A new hybrid system capable of efficient lentiviral vector production and stable gene transfer mediated by a single helper-dependent adenoviral vector. *J Virol* 2003; 77: 2964–2971.
33. Okada T, Caplen NJ, Ramsey WJ, *et al.* In situ generation of pseudotyped retroviral progeny by adenovirus-mediated transduction of tumor cells enhances the killing effect of HSV-tk suicide gene therapy in vitro and in vivo. *J Gene Med* 2004; **6**: 288–299.
34. Sclimenti CR, Thyagarajan B, Calos MP. Directed evolution of a recombinase for improved genomic integration at a native human sequence. *Nucleic Acids Res* 2001; **29**: 5044–5051.
35. Anson DS. The use of retroviral vectors for gene therapy – what are the risks? A review of retroviral pathogenesis and its relevance to retroviral vector-mediated gene delivery. *Genet Vaccines Ther* 2004; **2**: 9.
36. Smith MC, Thorpe HM. Diversity in the serine recombinases. *Mol Microbiol* 2002; 44: 299–307.

Important Role of Endogenous Erythropoietin System in Recruitment of Endothelial Progenitor Cells in Hypoxia-Induced Pulmonary Hypertension in Mice

Kimio Satoh, MD; Yutaka Kagaya, MD, PhD; Makoto Nakano, MD; Yoshitaka Ito, MD; Jun Ohta, MD, PhD; Hiroko Tada, MD, PhD; Akihiko Karibe, MD, PhD; Naoko Minegishi, MD, PhD; Norio Suzuki, PhD; Masayuki Yamamoto, MD, PhD; Masao Ono, MD, PhD; Jun Watanabe, MD, PhD; Kunio Shirato, MD, PhD; Naoto Ishii, MD, PhD; Kazuo Sugamura, MD, PhD; Hiroaki Shimokawa, MD, PhD

Background—Recent studies have suggested that endogenous erythropoietin (Epo) plays an important role in the mobilization of bone marrow–derived endothelial progenitor cells (EPCs). However, it remains to be elucidated whether the Epo system exerts protective effects on pulmonary hypertension (PH), a fatal disorder encountered in cardiovascular medicine.

Methods and Results—A mouse model of hypoxia-induced PH was used for study. We evaluated right ventricular systolic pressure, right ventricular hypertrophy, and pulmonary vascular remodeling in mice lacking the Epo receptor (EpoR) in nonerythroid lineages ($EpoR^{-/-}$ rescued mice) after 3 weeks of exposure to hypoxia. Those mice lack EpoR in the cardiovascular system but not in the hematopoietic system. The development of PH and pulmonary vascular remodeling were accelerated in $EpoR^{-/-}$ rescued mice compared with wild-type mice. The mobilization of EPCs and their recruitment to the pulmonary endothelium were significantly impaired in $EpoR^{-/-}$ rescued mice. By contrast, reconstitution of the bone marrow with wild-type bone marrow cells ameliorated PH in the $EpoR^{-/-}$ rescued mice. Hypoxia enhanced the expression of EpoR on pulmonary endothelial cells in wild-type but not $EpoR^{-/-}$ rescued mice. Finally, hypoxia activated endothelial nitric oxide synthase in the lungs in wild-type mice but not in $EpoR^{-/-}$ rescued mice.

Conclusions—These results indicate that the endogenous Epo/EpoR system plays an important role in the recruitment of EPCs and prevents the development of PH during chronic hypoxia in mice in vivo, suggesting the therapeutic importance of the system for the treatment of PH. (***Circulation.* 2006;113:1442-1450.**)

Key Words: hypertension, pulmonary ■ hypoxia ■ endothelium ■ vasculature ■ remodeling

Erythropoietin (Epo) has long been regarded as a hypoxia-induced hormone that acts exclusively in the proliferation and differentiation of erythroid progenitors.[1] However, recent studies have demonstrated the expression of the Epo receptor (EpoR) in the cardiovascular system,[2,3] and the therapeutic potential of Epo has been noted in a variety of disorders, including cerebral infarction, myocardial ischemia/reperfusion, and congestive heart failure.[4–6] We also have recently demonstrated the protective role of endogenous Epo in patients with acute myocardial infarction.[7] However, the potential protective role of the endogenous Epo/EpoR system against pulmonary hypertension (PH) remains to be examined.

Clinical Perspective p 1450

Hypoxia has been considered to increase plasma levels of Epo and hematocrit, resulting in enhanced blood viscosity and PH.[8] However, exogenous Epo does not accelerate hypoxia-induced PH in rats.[9] Rather, Epo exerts direct protective effects on endothelial cells[10,11] and enhances the mobilization of endothelial progenitor cells (EPCs)[12] and their proliferative and adhesive capacity,[13] thus promoting endothelial repair and postnatal vasculogenesis.[14,15] Pulmonary endothelium is important in the maintenance of pulmonary vasculature,[16] whereas endothelial dysfunction accelerates pulmonary vascular remodeling in hypoxia-induced PH.[17] Therefore, it is conceivable that Epo has protective

Received August 18, 2005; revision received December 17, 2005; accepted January 20, 2006.

From the Departments of Cardiovascular Medicine (K. Satoh, Y.K., M.N., Y.I., J.O., H.T., A.K., J.W., K. Shirato, H.S.), Pathology (M.O.), and Microbiology and Immunology (N.I., K. Sugamura), Tohoku University Biomedical Engineering Research Organization (TUBERO) (N.M.), Tohoku University Graduate School of Medicine, Sendai, Japan, and the Center for Tsukuba Advanced Research Alliance (N.S., M.Y.), University of Tsukuba, Tsukuba, Japan.

Correspondence to Hiroaki Shimokawa, MD, PhD, Professor and Chairman, Department of Cardiovascular Medicine, Tohoku University Graduate School of Medicine, 1-1 Seiryo-machi, Aoba-ku, Sendai, 980-8574, Japan. E-mail shimo@cardio.med.tohoku.ac.jp

Circulation is available at http://www.circulationaha.org

DOI: 10.1161/CIRCULATIONAHA.105.583732

effects on pulmonary endothelial cells and inhibits the development of PH.

Hypoxia induces vascular endothelial growth factor (VEGF) and Epo,[18] thus promoting mobilization of EPCs and their homing to the ischemic tissue.[12,19] Recent studies have shown that intravenously injected EPCs home to pulmonary vasculature and ameliorate pulmonary vascular remodeling in monocrotaline-induced PH, demonstrating a potential role of exogenous EPCs as a source of pulmonary endothelial cells in vivo.[20,21] In the present study, we thus examined our hypothesis that the endogenous Epo/EpoR system plays an important protective role against the development of hypoxia-induced PH. For this purpose, we used EpoR-null mutant mice expressing EpoR exclusively in the erythroid lineage ($EpoR^{-/-}$ rescued mice).[22]

Methods

Animal Preparation

All procedures were performed according to the protocols approved by the Institutional Committee for Use and Care of Laboratory Animals of Tohoku University, Sendai, Japan. Because systemic deletion of EpoR is embryo-lethal,[1] we rescued these mice with the EpoR that is exclusively expressed in erythroid progenitor cells under the regulatory domain of globin transcription factor 1 (GATA-1) ($EpoR^{-/-}$ rescued mice).[22,23] The detailed procedures used to generate these mice were as follows. First, EpoR cDNA was ligated to a genomic fragment containing the hematopoietic regulatory domain of GATA-1 (*GATA-1–HRD*), which regulates the expression of EpoR in the hematopoietic progenitors. Second, these *GATA-1–HRD-EpoR* constructs were applied to produce transgenic mice, which were mated with $EpoR^{+/-}$ mice to establish the compound mutant $EpoR^{+/-}$ mice: *GATA-1–HRD-EpoR*. Finally, $EpoR^{-/-}$ rescued mice were generated by crossing these compound mutant mice and $EpoR^{+/-}$ mice. The EpoR was expressed under the control of an erythroid-specific promoter in the $EpoR^{-/-}$ rescued mice[23]; therefore, the expression was limited to the erythroid-lineage cells. By contrast, endogenous expression of EpoR mRNA was detected in most of the nonerythroid tissues in wild-type mice.[22] Thus, $EpoR^{-/-}$ rescued mice are characterized by the absence of EpoR in the cardiovascular system but a normal hematopoietic system.

In the present study, a total of 120 male wild-type (C57BL/6) and 100 $EpoR^{-/-}$ rescued male mice (8 weeks old) were used. For the assessment of PH and histological evaluations, wild-type and $EpoR^{-/-}$ rescued mice were divided into 2 groups each (n=10 each for the 4 groups). One group was maintained in room air (21% O_2), and the other group was exposed to hypoxia (10% O_2) for 3 weeks. For Kaplan-Meier analysis, additional groups of mice were used (n=15 each for the 4 groups).

Bone Marrow Transplantation

Transgenic mice constitutively expressing green fluorescent protein (GFP) under the transcriptional regulation of an endothelial cell–specific promoter (Tie2-GFP mice) were obtained from Jackson Laboratory (Bar Harbor, Me). Bone marrow transplantation was performed as previously described.[15] Briefly, recipient mice were lethally irradiated and received an intravenous injection of 5×10^6 donor bone marrow cells suspended in 100 μL calcium- and magnesium-free phosphate-buffered saline with 2% fetal bovine serum (FBS). Six weeks after the transplantation, these mice were transferred to hypoxic chambers (10% O_2) and were maintained for 3 weeks as previously described.[24]

Measurements

Mice were anesthetized with an intraperitoneal injection of ketamine (60 mg/kg) and xylazine (8 mg/kg). Right ventricular systolic pressure (RVSP) was measured by insertion of a 25-gauge needle connected to a pressure transducer. Hematocrit was measured by use of an automatic hemocytometer (Nihon-Kohden, Tokyo, Japan). For morphometric analysis, tissue sections were prepared from the formalin-fixed and paraffin-embedded left lung, stained with elastica Masson, and assessed by microscopy. Pulmonary arteries adjacent to an airway distal to the respiratory bronchiole were evaluated as previously reported in a modified protocol.[25] Briefly, the arteries were considered muscularized if they had a distinct double elastic lamina visible for at least half the diameter in the vessel cross section. The percentage of vessels with double elastic lamina was calculated as the number of muscularized vessels per total number of vessels counted. In each section, a total of 60 vessels were examined by use of a computer-assisted imaging system (DXM1200 with ACT-1 software, Nikon, Tokyo, Japan). This analysis was performed separately for different categories (external diameters, 25 to 60 μm and 60 to 100 μm). For immunohistological staining, monoclonal antibody to α-smooth muscle actin (αSMA, 1:300, DAKO, Denmark) was used as the primary antibody.

Immunofluorescence Staining

Immunofluorescence staining was performed on 4% paraformaldehyde–fixed frozen sections. The primary antibodies used were anti-EpoR (1:50, Santa Cruz Biotechnology, Inc, Santa Cruz, Calif), anti-mouse CD31 (1:400, BD PharMingen, San Diego, Calif), and anti-GFP (1:1000, Molecular Probes). Subsequently, Alexa Fluor 488– or Alexa Fluor 594–labeled secondary antibodies and Prolong antifade reagent with DAPI (Molecular Probes) were used. As a negative control, species- and isotype-matched immunoglobulin G was used in place of the primary antibody. Slides were viewed with a confocal fluorescence microscope (Fluoview FV1000, Olympus, Tokyo, Japan).

Flow Cytometry and EPC Culture Assay

Peripheral blood mononuclear cells (PBMCs) were isolated by density gradient centrifugation with Nycoprep Animal 1.077 (Axis-Shield). To quantify the number of $Flk\text{-}1^+/CD133^+$ cells, we used phycoerythrin-labeled anti-mouse Flk-1, FITC-labeled anti-mouse CD133 (eBioscience, San Diego, Calif), and biotinylated anti-mouse lineage antibodies (Mac-1, Gr-1, B220, CD4, CD8, and Ter119, BD PharMingen).[12] Quantitative analysis was performed by a fluorescence-activated cell sorter (FACScalibur, Becton Dickinson, San Jose, Calif). For EPC culture, isolated PBMCs (5×10^6 cells per well) were suspended in Medium-199 supplemented with 20% FBS, brain pituitary extract, antibiotics, 100 ng/mL VEGF, and 50 ng/mL basic fibroblast growth factor (R&D Systems, Minneapolis, Minn) and cultured on fibronectin-coated chamber slides (BioCoat, Becton Dickinson) for 7 days.[12,26] To confirm the incorporation of 1,1′-dioctadecyl-3,3,3′,3′-tetramethylindocarbocyanine perchlorate (DiI)-labeled acetylated LDL (DiI-AcLDL), cultured cells were incubated in medium containing 2 μg/mL DiI-AcLDL (Molecular Probes) for 3 hours at 37°C. Endothelium-like cells were identified by the uptake of DiI-AcLDL and Flk-1 expression.[12] The expression of EpoR on endothelium-like cells was confirmed by double staining with biotinylated anti-mouse EpoR antibodies (1:50, R&D Systems) and anti-Flk-1 (VEGF receptor-2, 1:200, Santa Cruz Biochemicals).[26] Endothelium-like cells (1×10^6 cells per mouse) were labeled with CellTracker CM-DiI (Molecular Probes, Eugene, Ore),[26] suspended in 100 μL calcium- and magnesium-free phosphate-buffered saline with 2% FBS, and injected into the tail vein of hypoxic mice.

Western Blotting

Cell lysates from lung homogenates were separated by sodium dodecyl sulfate–polyacrylamide gel electrophoresis and transferred onto polyvinylidene difluoride membranes (Millipore). Subsequently, the membranes were probed with antibodies to mouse EpoR (Santa Cruz Biochemicals), endothelial nitric oxide synthase (eNOS, BD Biosciences), and β-actin (Cell Signaling, Danvers, Mass). Signals were visualized by the ECL detection system (Amersham Biosciences, Uppsala, Sweden).

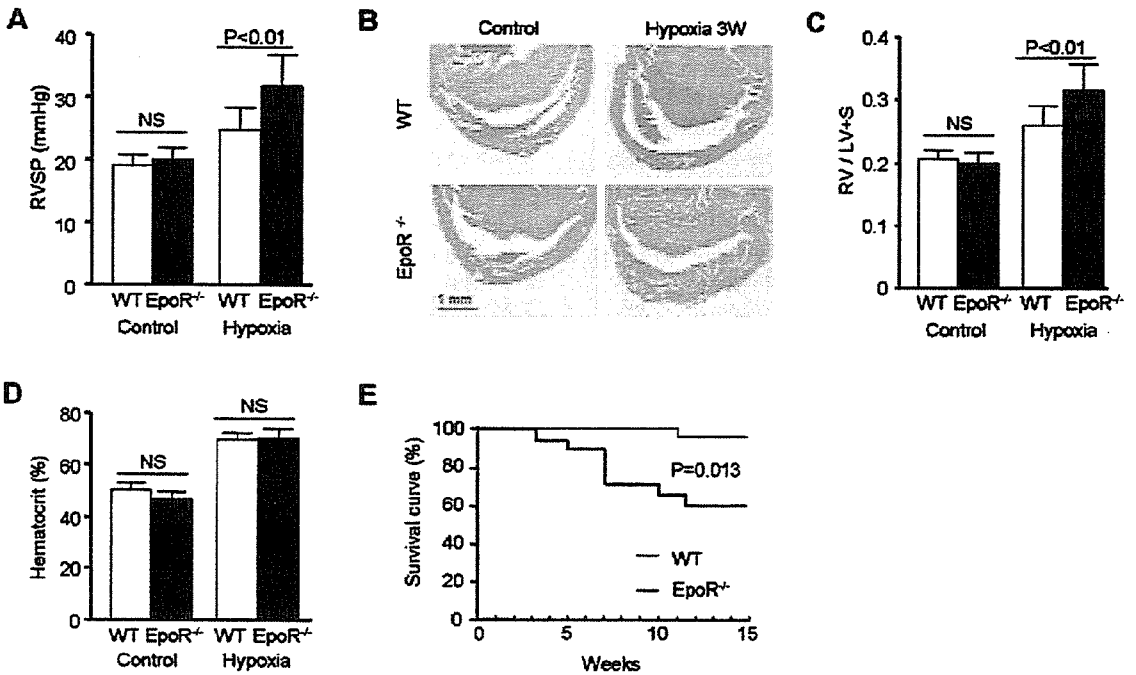

Figure 1. EpoR deficiency accelerates hypoxia-induced PH. Shown are effects of EpoR deficiency and chronic hypoxia on RVSP. A, RVH (weight ratio of right ventricle to left ventricle plus septum [RV/LV+S], B and C), and hematocrit (D) in mice (n=10 each for panels A through C, and n=5 each for panel D). WT indicates wild-type mice; EpoR$^{-/-}$, EpoR$^{-/-}$ rescued mice; control, normoxic mice; and hypoxia, mice exposed to 3 weeks of hypoxia (10% O_2). Results are expressed as mean±SD. E, Survival curves under chronic hypoxia (n=15 each).

Statistical Analysis

Quantitative results were expressed as mean±SD. Comparisons of parameters among the 2 or 3 groups were made by 1-way analysis of variance, and comparisons of the different oxygen conditions of parameters between the 2 genotypes were made by 2-way analysis of variance, followed by a post hoc analysis using the Bonferroni test. The Kaplan-Meier method was used to make survival curves, and the survival curves were compared by use of the log-rank test. A value of $P<0.05$ was considered to be statistically significant. Statistical analyses were performed by use of the StatView statistical package (StatView 5.0, SAS Institute Inc).

The authors had full access to the data and take full responsibility for its integrity. All authors have read and agree to the article as written.

Results

EpoR Deficiency Promotes PH and Pulmonary Vascular Remodeling

Under normoxic conditions, RVSP and right ventricular hypertrophy (RVH) were comparable between wild-type and EpoR$^{-/-}$ rescued mice (Figure 1A–1C). However, after the exposure to hypoxia (10% O_2 for 3 weeks), RVSP was significantly higher and RVH was more accelerated in EpoR$^{-/-}$ rescued mice (Figure 1A through 1C), whereas the hematocrit was comparable between the 2 groups (Figure 1D). In addition, survival was significantly impaired in EpoR$^{-/-}$ rescued mice under chronic hypoxia (Figure 1E). In both groups, most animals that died showed ascites, RVH, and dilatation, suggesting that the main cause of death was right ventricular failure.

Histological examination showed that in wild-type mice, chronic hypoxia caused small-vessel muscularization, whereas in EpoR$^{-/-}$ rescued mice (although the extent of muscularization under normoxia was similar to that found in wild-type mice), the hypoxia-induced muscularization was significantly accelerated (Figures 2 and 3). Immunostaining of lung sections showed that the hyperplastic cell population consisted of smooth muscle cells, inasmuch as they expressed αSMA (Figure 2).

Impaired Mobilization of EPCs in EpoR$^{-/-}$ Rescued Mice

To compare the effect of hypoxia on the mobilization of EPCs between wild-type and EpoR$^{-/-}$ rescued mice, fluorescence-activated cell sorter analysis was performed in the peripheral blood. The number of EPCs, when defined as Flk-1$^+$/CD133$^+$ cells in PBMCs,[27,28] was significantly increased under hypoxic conditions in wild-type mice but not in EpoR$^{-/-}$ rescued mice (Figure 4A). Similarly, hypoxia significantly increased the number of DiI-AcLDL$^+$/Flk-1$^+$ endothelium-like cells cultivated from PBMCs in wild-type mice but not in EpoR$^{-/-}$ rescued mice (Figure 4B). Importantly, cultivated endothelium-like cells from wild-type mice expressed EpoR; however, this was not the case for the cells from EpoR$^{-/-}$ rescued mice (Figure 4C). To further confirm the incorporation of bone marrow–derived endothelium-like cells into the pulmonary vessels, endothelium-like cells cultivated from mononuclear cells were intravenously injected into the wild-type mice that had already been exposed to hypoxia (10% O_2) for 7 days. After additional exposure to hypoxia for 7 days, incorporation of the injected cells into the pulmonary endothelium was assessed by confocal micros-

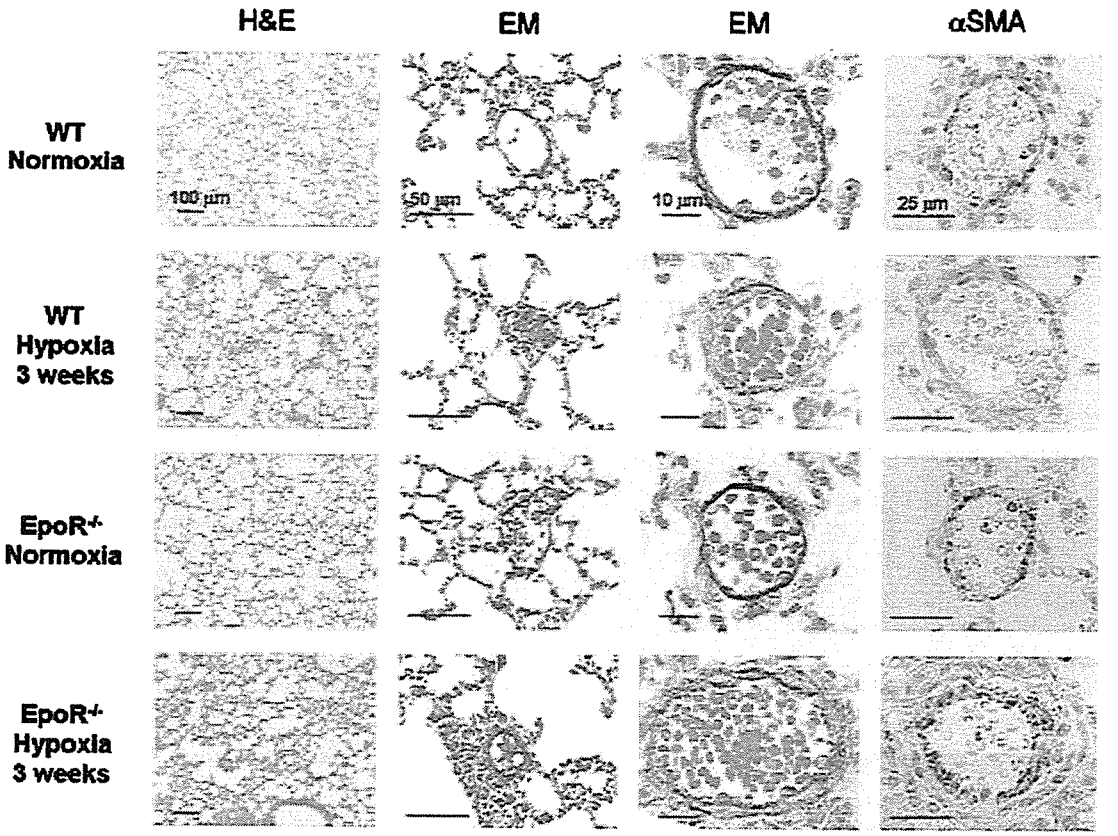

Figure 2. EpoR deficiency accelerates hypoxia-induced pulmonary vascular remodeling. Sections stained with hematoxylin and eosin (H&E) at low magnification and elastica Masson (EM) staining at intermediate magnification show the morphological changes in lungs. At high-power magnification, the development of pulmonary vascular remodeling is shown by EM staining or by immunostaining for αSMA.

copy (Figure 4D). Actual incorporation of infused cells from wild-type and EpoR$^{-/-}$ rescued mice into pulmonary endothelial cells was confirmed by immunostaining for CD31. Importantly, the number of the CD31-positive cells migrating to the pulmonary endothelium was significantly less in the cells from EpoR$^{-/-}$ rescued mice than in cells from wild-type mice (Figure 4E).

Bone Marrow–Derived EPCs Incorporated Into Pulmonary Endothelium Inhibit Development of PH

To confirm the incorporation of bone marrow–derived EPCs into pulmonary vessels in vivo, wild-type mice were lethally irradiated, transplanted with bone marrow cells from Tie2-GFP transgenic mice, and bred under hypoxic conditions. After 3 weeks of hypoxia, we found that GFP-positive endothelial cells were incorporated into the pulmonary endothelium (Figure 5A). The number of the GFP-positive endothelial cells that were incorporated into the pulmonary endothelium was significantly increased by hypoxic exposure compared with control conditions (Figure 5B).

To further examine whether the impaired mobilization and incorporation of bone marrow–derived EPCs in EpoR$^{-/-}$ rescued mice was involved in the development of severe PH,

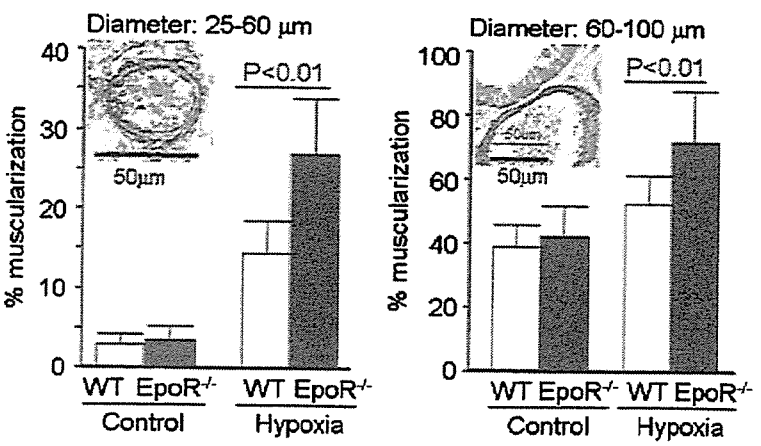

Figure 3. EpoR deficiency and hypoxia accelerate the degree of muscularization in pulmonary small vessels in mice. In each animal, 60 vessels were counted per lung section (n=6 each). Representative pictures of muscularized small vessels with double elastic lamina are shown in each panel. Results are expressed as mean±SD.

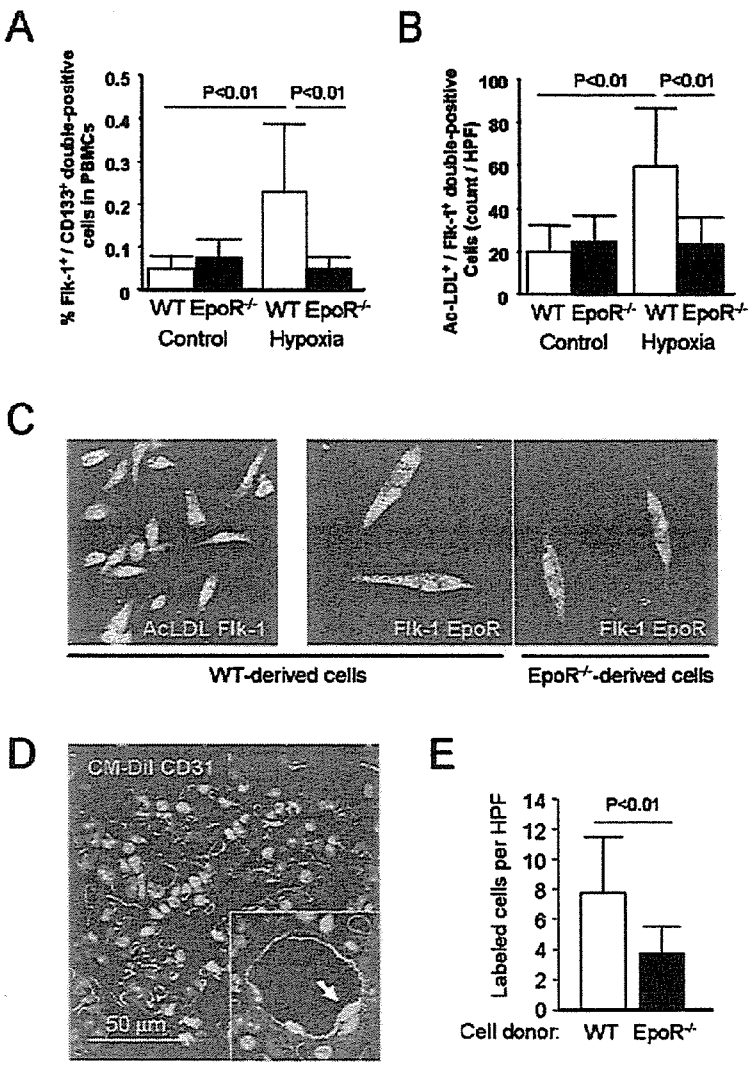

Figure 4. In vivo recruitment of EPCs into the circulation is impaired in EpoR$^{-/-}$ mice. A and B, Hypoxia (10% O_2 for 7 days) significantly increased the number of Flk-1$^+$/CD133$^+$ cells in the PBMCs (n=8 each, A) and the number of DiI-AcLDL$^+$/Flk-1$^+$ double-positive cells (endothelium-like cells) in WT mice, but not in EpoR$^{-/-}$ mice (n=6 each, B). HPF indicates high-power field. C, Endothelium-like cells were identified by the uptake of DiI-labeled AcLDL (red) and the staining with Flk-1 (green). The expression of EpoR (red) was observed only in the cells from WT mice but not in those from EpoR$^{-/-}$ mice. D, Shown is the incorporation of injected cells (1×10^6 cells per mouse) into the pulmonary endothelium on day 7 of hypoxic exposure (arrow). E, The number of incorporated cells was significantly reduced in EpoR$^{-/-}$ mice. In each animal, 10 different sections were observed. Results are expressed as mean±SD.

EpoR$^{-/-}$ rescued mice were lethally irradiated and then transplanted with bone marrow cells from wild-type or EpoR$^{-/-}$ rescued mice. As a control, wild-type mice reconstituted with wild-type bone marrow cells were prepared. After 6 weeks, these mice were exposed to hypoxia for 3 weeks. Hemodynamic analysis revealed that the development of PH, when assessed by RVSP and RVH, was partially ameliorated in EpoR$^{-/-}$ rescued mice transplanted with wild-type bone marrow cells (Figure 5C). Furthermore, the degree of pulmonary vessel muscularization (diameter, 25 μm to 60 μm) was also ameliorated in this group, whereas hematocrit values were comparable among the 3 groups (Figure 5D).

Impaired Response of Pulmonary Endothelial Cells in EpoR$^{-/-}$ Rescued Mice

To further elucidate any other mechanism that promotes PH in EpoR$^{-/-}$ rescued mice, we focused on the response of pulmonary endothelial cells to hypoxic exposure. The expression of EpoR was absent in pulmonary endothelial cells from EpoR$^{-/-}$ rescued mice, whereas the expression was enhanced by hypoxic exposure in wild-type mice (Figure 6). Moreover, because chronic hypoxia has been reported to increase eNOS protein in rat lungs,[29] we evaluated the expression of eNOS. After 3 weeks of hypoxia, lung eNOS protein expression was increased in wild-type mice but not in EpoR$^{-/-}$ rescued mice (Figure 7).

Discussion

The novel finding of the present study is that the mobilization of EPCs from the bone marrow and their incorporation into the pulmonary endothelium are impaired in EpoR$^{-/-}$ rescued mice, with a resultant potentiation of PH and pulmonary vascular remodeling in response to chronic hypoxia. To the best of our knowledge, this is the first study demonstrating that the endogenous Epo/EpoR system exerts protective effects on pulmonary endothelium and its progenitors and inhibits the development of hypoxia-induced PH.

Epo Mobilizes EPCs and Repairs Pulmonary Endothelium

In the present study, ex vivo–cultivated peripheral blood–derived EPCs showed the expression of EpoR in wild-type mice but not in EpoR$^{-/-}$ rescued mice. The lack of an effect of Epo may involve the progression of pulmonary vascular

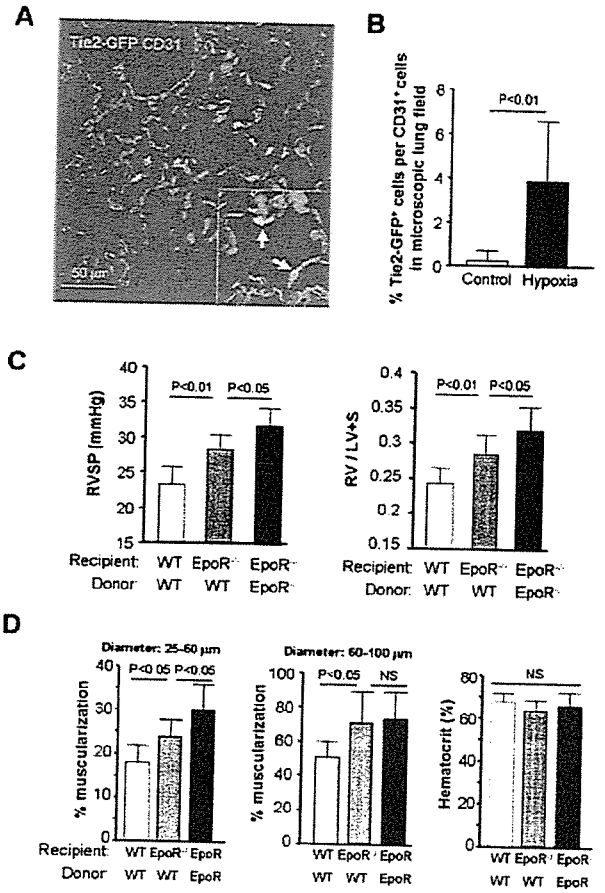

Figure 5. Bone marrow–derived EPCs incorporate into pulmonary endothelium and inhibit the development of hypoxia-induced PH. A, Bone marrow–derived endothelial cells were identified by the expression of endothelium-specific expression of Tie2-GFP (green) and staining with CD31 (red). High-power magnification revealed incorporated cells that were positive for both GFP and CD31 (arrows). B, Percentages of the number of GFP^+ cells per $CD31^+$ endothelial cells in the lung field were assessed. In each animal, 5 different sections were observed. C, After 3 weeks of hypoxia, hemodynamic analysis revealed the amelioration of PH assessed by RVSP and RVH in $EpoR^{-/-}$ mice transplanted with WT bone marrow cells. D, The degree of small (25- to 60-μm) vessel muscularization was reduced by the WT bone marrow, whereas the hematocrit level was comparable after 3 weeks of hypoxia. In each animal, 60 vessels were counted per mouse lung section. Shown are WT mice reconstituted with WT bone marrow (open columns, n=8) and $EpoR^{-/-}$ mice reconstituted with WT bone marrow (gray columns, n=8) or $EpoR^{-/-}$ bone marrow (closed columns, n=8). Results are expressed as mean±SD.

remodeling that is due to impairment in the mobilization of EPCs and their recruitment to the injured pulmonary endothelium. This notion is supported by the present in vivo findings. Indeed, mobilization of EPCs, defined as $Flk\text{-}1^+/CD133^+$ cells in the peripheral blood and EPC culture assay, was impaired in $EpoR^{-/-}$ rescued mice. Intravenously infused bone marrow–derived EPCs were incorporated into the pulmonary endothelium; this process was significantly impaired in the EPCs from $EpoR^{-/-}$ rescued mice. Moreover, GFP-positive cells were incorporated into the pulmonary endothelium in chimeric mice that were reconstituted with bone marrow cells from Tie2-GFP transgenic mice. The expression of GFP is regulated by the Tie2 promoter and therefore identifies bone marrow–derived differentiated endothelial cells and EPCs.[15] These findings are in line with findings in previous studies showing that circulating EPCs contribute to the endogenous vascular repair process and play an important role in inhibiting vascular remodeling.[30] In addition, Davie et al[31] demonstrated the incorporation of c-kit–positive progenitor cells into the pulmonary vessels under hypoxic conditions. Although the number of bone marrow–derived endothelial cells in the lung field was relatively small (≈3% to 5%) compared with that in the hind-limb ischemia or tumor angiogenesis model,[14,32] bone marrow–derived cells are likely to contribute to pulmonary endothelial repair not only by incorporating into the endothelial cells but also by improving the functions of the resident pulmonary endothelial cells through paracrine effects.[33] EPCs also are reported to express eNOS and produce nitric oxide (NO).[34] Indeed, the concept that bone marrow–derived endothelial cells could repair the pulmonary endothelium and ameliorate PH, especially through paracrine effects, has recently been proposed.[20,21] By contrast, defective mobilization and recruitment of EPCs in $EpoR^{-/-}$ rescued mice may lead to the potentiation of PH in response to chronic hypoxia. Indeed, it has been recently reported that the number of circulating EPCs is associated with endothelial dysfunction in humans.[35] Taken together, Epo may serve as a cytokine that elicits EPC mobilization, promoting the repair process of the injured pulmonary endothelium and thus inhibiting the development of PH.

Epo Has Direct Protective Effects on Pulmonary Endothelial Cells

Antiinflammatory and antiapoptotic effects on pulmonary endothelial cells have been shown to prevent the development of PH in rats.[36,37] In line with these findings, we observed that lack of EpoR expression on pulmonary endothelium accelerates pulmonary vascular remodeling in $EpoR^{-/-}$ rescued mice; this occurrence may be partly due to the lack of direct effects of Epo on pulmonary endothelial cells.[38–40] By contrast, the expression of EpoR was upregulated by hypoxia in wild-type mice. A similar observation has been previously reported with regard to human umbilical vein endothelial cells in vitro, where EpoR expression was induced by Epo and hypoxia.[41] Moreover, parallel increases in eNOS expression and NO production in response to Epo were observed during hypoxia.[41] An increase in the plasma level of Epo under hypoxic conditions combined with an upregulation of EpoR on pulmonary endothelial cells may augment the endothelial responses. In addition, the induction of eNOS and increased endothelial NO production by Epo may allow the pulmonary vasculature to recover blood flow and ameliorate PH.[42] Importantly, these endothelial responses were absent in $EpoR^{-/-}$ rescued mice with accelerated PH and pulmonary vascular remodeling. Taken together, Epo has direct effects on pulmonary endothelial cells in addition to indirect effects on the recruitment of cells from bone marrow. All these effects of Epo may help to protect and maintain endothelial function and to inhibit pulmonary vascular remodeling under chronic hypoxia.

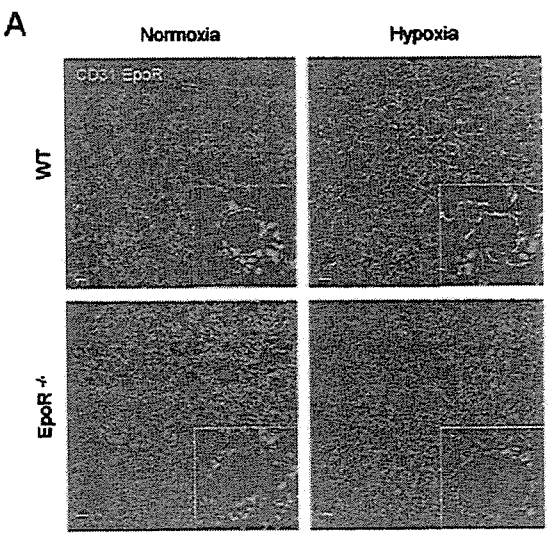

Figure 6. Hypoxia enhances the expression of EpoR on pulmonary endothelial cells. A, Representative lung sections from normoxic and hypoxic mice. Hypoxia enhanced the expression of EpoR (green) in WT mice but not in EpoR$^{-/-}$ mice. Bar, 50 μm. B, Western blot analysis of EpoR in lung homogenates of WT mice after 3 weeks of hypoxia (10% O_2, n=10 each). Results are expressed as mean±SD.

Limitations of the Present Study

Several limitations should be mentioned for the present study. First, the hypoxia-induced PH model may not fully represent primary PH in humans because this model shows a considerably high hematocrit and blood viscosity.[16] Epo has been thought to increase these parameters, with a resultant development of PH.[8] However, in the present study, RVSP and RVH were accelerated in EpoR$^{-/-}$ rescued mice in response to chronic hypoxia compared with wild-type mice, despite the comparable increase in hematocrit between the 2 strains. Furthermore, it has previously been shown that pulmonary arterial pressure and RVH are not increased in Epo-treated rats despite a significant increase in hematocrit and blood viscosity.[43] Taken together, these results suggest that hypoxia-induced PH cannot be explained by simple polycythemia. Second, the mechanisms for the beneficial effects of Epo have been examined in only 1 model (hypoxia-induced PH) by comparing wild-type and EpoR$^{-/-}$ rescued mice. Thus, the importance of the endogenous Epo/EpoR system should be confirmed in other PH models with different etiologies (eg, bone morphogenetic protein receptor-2 [BMPR2]–heterozygous mutant [*BMPR2*$^{+/-}$] mice[44]), although the same mechanisms for the protective effects of the Epo/EpoR system may be expected, especially when nonerythropoietic derivatives of Epo are used.[45]

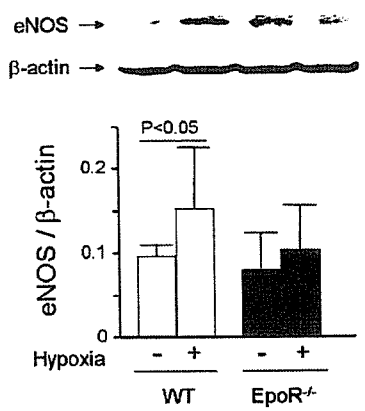

Figure 7. Western blot analysis of eNOS in the lung. The expression of eNOS was upregulated in WT but not EpoR$^{-/-}$ mice after 3 weeks of hypoxia (10% O_2, n=10 each). Results are expressed as mean±SD.

Clinical Implications and Conclusions

In the present study, we were able to demonstrate that the endogenous Epo/EpoR system exerts important protective effects against the development of hypoxia-induced PH through mobilization of bone marrow–derived EPCs and stimulation of preexisting pulmonary endothelial cells. This is in line with our recent finding of the protective role of the endogenous Epo system in patients with acute myocardial infarction.[7] Indeed, recent studies have shown that Epo increases the number of EPCs in humans[46] and that Epo has an ischemia-induced angiogenic potential during retinal angiogenesis in diabetic patients.[47] Therefore, the present findings suggest that the therapeutic use of Epo might be useful for the treatment of human diseases.[48] However, further careful considerations should be made before Epo is applied in the clinical setting.

In conclusion, the present study demonstrates an important protective role of the endogenous Epo/EpoR system in the mobilization and incorporation of EPCs into the pulmonary endothelium and in the maintenance of pulmonary endothelial integrity in the pathogenesis of hypoxia-induced PH.

Acknowledgments

This study was supported in part by grants-in-aid for scientific research from the Ministry of Education, Culture, Sports, Science and Technology, Tokyo, Japan (16209027, 16659192), the Japanese Ministry of Health, Labor, and Welfare, Tokyo, Japan, and the Japan Foundation of Cardiovascular Research, Tokyo, Japan.

Disclosures

None.

References

1. Wu H, Liu X, Jaenisch R, Lodish HF. Generation of committed erythroid BFU-E and CFU-E progenitors does not require erythropoietin or the erythropoietin receptor. *Cell*. 1995;83:59–67.

2. Anagnostou A, Liu Z, Steiner M, Chin K, Lee ES, Kessimian N, Noguchi CT. Erythropoietin receptor mRNA expression in human endothelial cells. *Proc Natl Acad Sci U S A*. 1994;91:3974–3978.
3. Wright GL, Hanlon P, Amin K, Steenbergen C, Murphy E, Arcasoy MO. Erythropoietin receptor expression in adult rat cardiomyocytes is associated with an acute cardioprotective effect for recombinant erythropoietin during ischemia-reperfusion injury. *FASEB J*. 2004;18:1031–1033.
4. Sadamoto Y, Igase K, Sakanaka M, Sato K, Otsuka H, Sakaki S, Masuda S, Sasaki R. Erythropoietin prevents place navigation disability and cortical infarction in rats with permanent occlusion of the middle cerebral artery. *Biochem Biophys Res Commun*. 1998;253:26–32.
5. Calvillo L, Latini R, Kajstura J, Leri A, Anversa P, Ghezzi P, Salio M, Cerami A, Brines M. Recombinant human erythropoietin protects the myocardium from ischemia-reperfusion injury and promotes beneficial remodeling. *Proc Natl Acad Sci U S A*. 2003;100:4802–4806.
6. Silverberg DS, Wexler D, Blum M, Keren G, Sheps D, Leibovitch E, Brosh D, Laniado S, Schwartz D, Yachnin T, Shapira I, Gavish D, Baruch R, Koifman B, Kaplan C, Steinbruch S, Iaina A. The use of subcutaneous erythropoietin and intravenous iron for the treatment of the anemia of severe, resistant congestive heart failure improves cardiac and renal function and functional cardiac class, and markedly reduces hospitalizations. *J Am Coll Cardiol*. 2000;35:1737–1744.
7. Namiuchi S, Kagaya Y, Ohta J, Shiba N, Sugi M, Oikawa M, Kunii H, Yamao H, Komatsu N, Yui M, Tada H, Sakuma M, Watanabe J, Ichihara T, Shirato K. High serum erythropoietin level is associated with smaller infarct size in patients with acute myocardial infarction who undergo successful primary percutaneous coronary intervention. *J Am Coll Cardiol*. 2005;45:1406–1412.
8. Hasegawa J, Wagner KF, Karp D, Li D, Shibata J, Heringlake M, Bahlmann L, Depping R, Fandrey J, Schmucker P, Uhlig S. Altered pulmonary vascular reactivity in mice with excessive erythrocytosis. *Am J Respir Crit Care Med*. 2004;169:829–835.
9. Petit RD, Warburton RR, Ou LC, Brinck-Johnson T, Hill NS. Exogenous erythropoietin fails to augment hypoxic pulmonary hypertension in rats. *Respir Physiol*. 1993;91:271–282.
10. Carlini RG, Dusso AS, Obialo CI, Alvarez UM, Rothstein M. Recombinant human erythropoietin (rHuEPO) increases endothelin-1 release by endothelial cells. *Kidney Int*. 1993;43:1010–1014.
11. Haller H, Christel C, Dannenberg L, Thiele P, Lindschau C, Luft FC. Signal transduction of erythropoietin in endothelial cells. *Kidney Int*. 1996;50:481–488.
12. Heeschen C, Aicher A, Lehmann R, Fichtlscherer S, Vasa M, Urbich C, Mildner-Rihm C, Martin H, Zeiher AM, Dimmeler S. Erythropoietin is a potent physiologic stimulus for endothelial progenitor cell mobilization. *Blood*. 2003;102:1340–1346.
13. George J, Goldstein E, Abashidze A, Wexler D, Hamed S, Shmilovich H, Deutsch V, Miller H, Keren G, Roth A. Erythropoietin promotes endothelial progenitor cell proliferative and adhesive properties in a PI 3-kinase–dependent manner. *Cardiovasc Res*. 2005;68:299–306.
14. Asahara T, Murohara T, Sullivan A, Silver M, van der Zee R, Li T, Witzenbichler B, Schatteman G, Isner JM. Isolation of putative progenitor endothelial cells for angiogenesis. *Science*. 1997;275:964–967.
15. Asahara T, Masuda H, Takahashi T, Kalka C, Pastore C, Silver M, Kearne M, Magner M, Isner JM. Bone marrow origin of endothelial progenitor cells responsible for postnatal vasculogenesis in physiological and pathological neovascularization. *Circ Res*. 1999;85:221–228.
16. Voelkel NF, Tuder RM. Hypoxia-induced pulmonary vascular remodeling: a model for what human disease? *J Clin Invest*. 2000;106:733–738.
17. Steudel W, Scherrer-Crosbie M, Bloch KD, Weimann J, Huang PL, Jones RC, Picard MH, Zapol WM. Sustained pulmonary hypertension and right ventricular hypertrophy after chronic hypoxia in mice with congenital deficiency of nitric oxide synthase 3. *J Clin Invest*. 1998;101:2468–2477.
18. Semenza GL, Wang GL. A nuclear factor induced by hypoxia via de novo protein synthesis binds to the human erythropoietin gene enhancer at a site required for transcriptional activation. *Mol Cell Biol*. 1992;12:5447–5454.
19. Asahara T, Takahashi T, Masuda H, Kalka C, Chen D, Iwaguro H, Inai Y, Silver M, Isner JM. VEGF contributes to postnatal neovascularization by mobilizing bone marrow–derived endothelial progenitor cells. *EMBO J*. 1999;18:3964–3972.
20. Nagaya N, Kangawa K, Kanda M, Uematsu M, Horio T, Fukuyama N, Hino J, Harada-Shiba M, Okumura H, Tabata Y, Mochizuki N, Chiba Y, Nishioka K, Miyatake K, Asahara T, Hara H, Mori H. Hybrid cell-gene therapy for pulmonary hypertension based on phagocytosing action of endothelial progenitor cells. *Circulation*. 2003;108:889–895.
21. Zhao YD, Courtman DW, Deng Y, Kugathasan L, Zhang Q, Stewart DJ. Rescue of monocrotaline-induced pulmonary arterial hypertension using bone marrow–derived endothelium-like progenitor cells: efficacy of combined cell and eNOS gene therapy in established disease. *Circ Res*. 2005;96:442–450.
22. Suzuki N, Ohneda O, Takahashi S, Higuchi M, Mukai HY, Nakahata T, Imagawa S, Yamamoto M. Erythroid-specific expression of the erythropoietin receptor rescued its null mutant mice from lethality. *Blood*. 2002;100:2279–2288.
23. Suzuki N, Suwabe N, Ohneda O, Obara N, Imagawa S, Pan X, Motohashi H, Yamamoto M. Identification and characterization of 2 types of erythroid progenitors that express GATA-1 at distinct levels. *Blood* 2003;102;3575–3583.
24. Katayose D, Ohe M, Yamauchi K, Ogata M, Shirato K, Fujita H, Shibahara S, Takishima T. Increased expression of PDGF A- and B-chain genes in rat lungs with hypoxic pulmonary hypertension. *Am J Physiol*. 1993;264:L100–L106.
25. Keegan A, Morecroft I, Smillie D, Hicks MN, MacLean MR. Contribution of the 5-HT_{1B} receptor to hypoxia-induced pulmonary hypertension: converging evidence using 5-HT_{1B}–receptor knockout mice and the 5-$HT_{1B/1D}$–receptor antagonist GR127935. *Circ Res*. 2001;89:1231–1239.
26. Aicher A, Heeschen C, Mildner-Rihm C, Urbich C, Ihling C, Technau-Ihling K, Zeiher AM, Dimmeler S. Essential role of endothelial nitric oxide synthase for mobilization of stem and progenitor cells. *Nat Med*. 2003;9:1370–1376.
27. Peichev M, Naiyer AJ, Pereira D, Zhu Z, Lane WJ, Williams M, Oz MC, Hicklin DJ, Witte L, Moore MA, Rafii S. Expression of VEGFR-2 and AC133 by circulating human $CD34^+$ cells identifies a population of functional endothelial precursors. *Blood*. 2000;95:952–958.
28. Urbich C, Dimmeler S. Endothelial progenitor cells: characterization and role in vascular biology. *Circ Res*. 2004;95:343–353.
29. Le Cras TD, Tyler RC, Horan MP, Morris KG, Tuder RM, McMurtry IF, Johns RA, Abman SH. Effects of chronic hypoxia and altered hemodynamics on endothelial nitric oxide synthase expression in the adult rat lung. *J Clin Invest*. 1998;101:795–801.
30. Iwakura A, Luedemann C, Shastry S, Hanley A, Kearney M, Aikawa R, Isner JM, Asahara T, Losordo DW. Estrogen-mediated, endothelial nitric oxide synthase–dependent mobilization of bone marrow–derived endothelial progenitor cells contributes to reendothelialization after arterial injury. *Circulation*. 2003;108:3115–3121.
31. Davie NJ, Crossno JT Jr, Frid MG, Hofmeister SE, Reeves JT, Hyde DM, Carpenter TC, Brunetti JA, McNiece IK, Stenmark KR. Hypoxia-induced pulmonary artery adventitial remodeling and neovascularization: contribution of progenitor cells. *Am J Physiol*. 2004;286:L668–L678.
32. Lyden D, Hattori K, Dias S, Costa C, Blaikie P, Butros L, Chadburn A, Heissig B, Marks W, Witte L, Wu Y, Hicklin D, Zhu Z, Hackett NR, Crystal RG, Moore MA, Hajjar KA, Manova K, Benezra R, Rafii S. Impaired recruitment of bone-marrow–derived endothelial and hematopoietic precursor cells blocks tumor angiogenesis and growth. *Nat Med*. 2001;7:1194–1201.
33. He T, Peterson TE, Katusic ZS. Paracrine mitogenic effect of human endothelial progenitor cells: role of interleukin-8. *Am J Physiol*. 2005;289:H968–H972.
34. Murohara T, Ikeda H, Duan J, Shintani S, Sasaki K, Eguchi H, Onitsuka I, Matsui K, Imaizumi T. Transplanted cord blood–derived endothelial precursor cells augment postnatal neovascularization. *J Clin Invest*. 2000;105:1527–1536.
35. Hill JM, Zalos G, Halcox JP, Schenke WH, Waclawiw MA, Quyyumi AA, Finkel T. Circulating endothelial progenitor cells, vascular function, and cardiovascular risk. *N Engl J Med*. 2003;348:593–600.
36. Abe K, Shimokawa H, Morikawa K, Uwatoku T, Oi K, Matsumoto Y, Hattori T, Nakashima Y, Kaibuchi K, Sueishi K, Takeshita A. Long-term treatment with a Rho-kinase inhibitor improves monocrotaline-induced fatal pulmonary hypertension in rats. *Circ Res*. 2004;94:385–393.
37. Itoh T, Nagaya N, Murakami S, Fujii T, Iwase T, Ishibashi-Ueda H, Yutani C, Yamagishi M, Kimura H, Kangawa K. C-type natriuretic peptide ameliorates monocrotaline-induced pulmonary hypertension in rats. *Am J Respir Crit Care Med*. 2004;170:1204–1211.
38. Dudley AC, Thomas DM, Best J, Jenkins A. A VEGF/JAK2/STAT5 axis may partially mediate endothelial cell tolerance to hypoxia. *Biochem J*. 2005;390:427–436.

39. Kano A, Wolfgang MJ, Gao Q, Jacoby J, Chai GX, Hansen W, Iwamoto Y, Pober JS, Flavell RA, Fu XY. Endothelial cells require STAT3 for protection against endotoxin-induced inflammation. *J Exp Med.* 2003; 198:1517–1525.
40. Silva M, Benito A, Sanz C, Prosper F, Ekhterae D, Nunez G, Fernandez-Luna JL. Erythropoietin can induce the expression of bcl-x(L) through Stat5 in erythropoietin-dependent progenitor cell lines. *J Biol Chem.* 1999;274:22165–22169.
41. Beleslin-Cokic BB, Cokic VP, Yu X, Weksler BB, Schechter AN, Noguchi CT. Erythropoietin and hypoxia stimulate erythropoietin receptor and nitric oxide production by endothelial cells. *Blood.* 2004; 104:2073–2080.
42. Champion HC, Bivalacqua TJ, D'Souza FM, Ortiz LA, Jeter JR, Toyoda K, Heistad DD, Hyman AL, Kadowitz PJ. Gene transfer of endothelial nitric oxide synthase to the lung of the mouse in vivo: effect on agonist-induced and flow-mediated vascular responses. *Circ Res.* 1999;84:1422–1432.
43. Petit RD, Warburton RR, Ou LC, Hill NS. Pulmonary vascular adaptations to augmented polycythemia during chronic hypoxia. *J Appl Physiol.* 1995;79:229–235.
44. Song Y, Jones JE, Beppu H, Keaney JF Jr, Loscalzo J, Zhang YY. Increased susceptibility to pulmonary hypertension in heterozygous BMPR2-mutant mice. *Circulation.* 2005;112:553–562.
45. Leist M, Ghezzi P, Grasso G, Bianchi R, Villa P, Fratelli M, Savino C, Bianchi M, Nielsen J, Gerwien J, Kallunki P, Larsen AK, Helboe L, Christensen S, Pedersen LO, Nielsen M, Torup L, Sager T, Sfacteria A, Erbayraktar S, Erbayraktar Z, Gokmen N, Yilmaz O, Cerami-Hand C, Xie QW, Coleman T, Cerami A, Brines M. Derivatives of erythropoietin that are tissue protective but not erythropoietic. *Science.* 2004;305:239–242.
46. Bahlmann FH, De Groot K, Spandau JM, Landry AL, Hertel B, Duckert T, Boehm SM, Menne J, Haller H, Fliser D. Erythropoietin regulates endothelial progenitor cells. *Blood.* 2004;103:921–926.
47. Watanabe D, Suzuma K, Matsui S, Kurimoto M, Kiryu J, Kita M, Suzuma I, Ohashi H, Ojima T, Murakami T, Kobayashi T, Masuda S, Nagao M, Yoshimura N, Takagi H. Erythropoietin as a retinal angiogenic factor in proliferative diabetic retinopathy. *N Engl J Med.* 2005;353: 782–792.
48. Maiese K, Li F, Chong ZZ. New avenues of exploration for erythropoietin. *JAMA.* 2005;293:90–95.

CLINICAL PERSPECTIVE

Pulmonary hypertension (PH) remains a fatal disorder encountered in cardiovascular medicine. Causes of the disorder include congestive heart failure, congenital heart disease, collagen disease, and primary PH. The increased pulmonary vascular resistance in PH is caused by the combined effects of enhanced pulmonary vascular tone, medial smooth muscle hypertrophy, and intimal thickening. Accumulating evidence indicates that vascular endothelial dysfunction is a key mechanism for the disorder. Erythropoietin (Epo) has long been thought to act exclusively on hematopoietic cells. However, recent studies have suggested that Epo also possesses several biological actions that protect vascular wall cells (including endothelial cells) that express the Epo receptor (EpoR). The endogenous Epo/EpoR system has been considered to play a role in the pathogenesis of PH in conjunction with polycythemia, with a resultant increase in pulmonary vascular resistance. However, our present study provides the novel concept that the pulmonary vascular Epo/EpoR system protects pulmonary endothelial cells directly (through the Epo/EpoR system) and indirectly (through the mobilization of bone marrow–derived endothelial progenitor cells), thus promoting pulmonary endothelial protection and repair. Our present study may have important clinical implications, inasmuch as we were able to demonstrate that the endogenous Epo/EpoR system exerts protective effects in PH and that Epo could be regarded as a new therapeutic tool for the treatment of the disorder. However, further studies are needed to confirm the therapeutic usefulness of Epo for the treatment of PH in humans.

OX40-OX40 Ligand Interaction through T Cell-T Cell Contact Contributes to CD4 T Cell Longevity[1]

Pejman Soroosh, Shouji Ine, Kazuo Sugamura, and Naoto Ishii[2]

Signals through the OX40 costimulatory receptor on naive CD4 T cells are essential for full-fledged CD4 T cell activation and the generation of CD4 memory T cells. Because the ligand for OX40 is mainly expressed by APCs, including activated B cells, dendritic cells, and Langerhans cells, the OX40-OX40 ligand (OX40L) interaction has been thought to participate in T cell-APC interactions. Although several reports have revealed the expression of OX40L on T cells, the functional significance of its expression on them is still unclear. In this study, we demonstrate that Ag stimulation induced an increase in the surface expression and transcript levels of OX40L in CD4 T cells. Upon contact with OX40-expressing T cells, the cell surface expression of OX40L on CD4 T cells was markedly down-regulated, suggesting that OX40-OX40L binding occurs through a novel T cell-T cell interaction. To investigate the function of this phenomenon, we examined the proliferative response and survival of OX40L-deficient CD4 T cells when challenged with Ag. In vitro studies demonstrated markedly less CD3-induced proliferation of OX40L-deficient CD4 T cells compared with wild-type CD4 T cells. When using TCR transgenic CD4 T cells upon Ag stimulation, survival of OX40L-deficient T cells was impaired. Furthermore, we show that upon antigenic stimulation, fewer OX40L-deficient CD4 T cells than wild-type cells survived following transfer into wild-type and sublethally irradiated recipient mice. Taken together, our findings indicate that OX40L-expressing T cells have an autonomous machinery that provides OX40 signals through a T cell-T cell circuit, creating an additional mechanism for sustaining CD4 T cell longevity. *The Journal of Immunology,* **2006, 176: 5975–5987.**

Optimal T cell activation requires not only signals delivered by Ag stimulation, but also costimulatory signals provided by APCs (1, 2). Although the interaction of CD28 with CD80/CD86 provides the best known costimulatory signals, other costimulatory molecules, including TNF superfamily molecules such as OX40 (CD134), CD27, and 4-1BB (CD137), can potently augment the full-fledged activation of T cells (3–5). Among these costimulatory molecules, OX40, which is transiently expressed by activated T cells, is not only essential for providing optimal CD4 T cell functioning (6–9), but also critically contributes to the generation of memory T cells by promoting the survival of effector T cells (10–12). The ligand for OX40 (OX40L)[3] is mainly expressed by APCs, such as activated B cells, dendritic cells (DCs), and Langerhans cells, as well as endothelial cells and T cells (13–21).

In several studies using OX40L-deficient mice, we and others have revealed that the absence of OX40L on APCs leads to a marked reduction in the proliferation and cytokine production of CD4 T cells (8, 9). We further showed that the effector function of encephalitogenic T cells transferred into OX40L-deficient mice could not be sustained in an experimental autoimmune encephalomyelitis system (22). Similarly, pathogenic T cells from mouse models of inflammatory bowel disease and graft-vs-host disease (GVHD) did not cause disease when they were transferred into OX40L-deficient recipient mice (23, 24), primarily because the donor T cells could not produce cytokines normally. These observations imply that OX40L expression, possibly by the APCs of recipient mice, is essential for donor CD4 T cell function.

Accumulating evidence, however, has shown that Ag-experienced T cells do express APC accessory molecules such as CD80, CD86, CD70, and CD40 (25–32). Bourgeois et al. (31) revealed that, upon activation, CD8 T cells endogenously express CD40, which can bind to CD40L on CD4 T cells through T cell-T cell interactions. The direct cross talk between CD4 and CD8 T cells consequently supports the generation of memory CD8 T cells in vivo. Little is known about whether other accessory molecules on T cells can provide efficient costimulatory signals during T cell-T cell interactions.

Our initial studies of OX40L revealed its up-regulation on HTLV-1-infected T cells (21). Several groups have shown that OX40L is also expressed on activated T cells (16, 18, 33, 34). More recently, in vitro studies demonstrated that T cells can acquire OX40L that apparently originates from OX40L-expressing cells in a non-Ag-specific manner (35, 36). In the present study, we set out to evaluate the expression and biological roles for the OX40L expressed on T cells. In this study, we document the endogenous expression of OX40L by activated CD4 T cells and reveal its costimulatory function in promoting CD4 T cell proliferation and survival through a novel CD4 T cell-T cell interaction.

Department of Microbiology and Immunology, Tohoku University Graduate School of Medicine, Sendai, Japan

Received for publication September 14, 2005. Accepted for publication February 27, 2006.

The costs of publication of this article were defrayed in part by the payment of page charges. This article must therefore be hereby marked *advertisement* in accordance with 18 U.S.C. Section 1734 solely to indicate this fact.

[1] This work was supported in part by a grant-in-aid for scientific research on priority areas from the Ministry of Education, Culture, Sports, Science, and Technology of Japan, and a grant-in-aid for scientific research on priority areas from the Japan Society for the Promotion of Science.

[2] Address correspondence and reprint requests to Dr. Naoto Ishii, Department of Microbiology and Immunology, Tohoku University Graduate School of Medicine, 2-1 Seiryo-machi, Aoba-ku, Sendai 980-8575 Japan. E-mail address: ishiin@mail.tains.tohoku.ac.jp

[3] Abbreviations used in this paper: OX40L, OX40 ligand; DC, dendritic cell; GVHD, graft-vs-host disease; KO, knockout.

0022-1767/06/$02.00

Materials and Methods

Mice

The OX40-deficient (OX40-knockout (KO)) and OX40L-deficient (OX40L-KO) mice were described previously (9, 16). Six- to 8-wk-old female C57BL/6 mice were purchased from Japan SLC. Ly-5.1$^+$ (CD45.1)-C57BL/6 mice were described previously (24). OT-II TCR transgenic mice were a gift from W. Heath (Walter and Eliza Hall Institute, Melbourne, Australia) and used as a source of Vα2$^+$Vβ5.1-2$^+$ CD4 T cells responsive to peptide 323–339 of OVA (37). OX40-KO, OX40L-KO, and Ly-5.1$^+$ OT-II TCR transgenic mice were generated in-house by intercrossing OT-II mice with OX40-KO, OX40L-KO, and Ly-5.1 mice, respectively. All of the mice used were on a C57BL/6 background, and they were bred and maintained under specific pathogen-free conditions in the Institute for Animal Experimentation, Tohoku University Graduate School of Medicine.

Cell lines

BW5147, a mouse thymoma cell line, was stably transfected with pCXN2-mOX40 expression plasmid, which carries the *chicken β-actin* promoter, followed by mouse *OX40* cDNA, yielding the BW-mOX40 line. BW-mOX40 cells and their parental BW5147 cells were maintained in RPMI 1640 medium supplemented with 10% FCS, 100 U/ml penicillin, and 100 μg/ml streptomycin.

Abs and flow cytometry

The following Abs were purchased from BD Biosciences: anti-CD3 FITC, anti-CD4 allophycocyanin, anti-CD8 allophycocyanin, anti-Vα2 PE, anti-Vβ5 FITC, anti-Ly-5.1 allophycocyanin, and anti-Ly-5.2 allophycocyanin. Anti-CD28 (eBioscience), control rat IgG (Cappel), and anti-CD3ε (2C11) were used for cell culture. Agonistic anti-mouse OX40 mAb (OX86) and inhibitory anti-OX40L mAb (MGP34) were used to stimulate and inhibit OX40 signals, respectively (24). Surface expression of OX40 and OX40L was detected with biotin-conjugated anti-OX40 and anti-OX40L mAbs, as briefly previously described (38). In brief, the cells were preincubated with excess rat Ig to block nonspecific binding of the labeled mAb and incubated with the labeled mAbs for 30 min at 4°C. Control staining for OX40 or OX40L was conducted in the presence of excess unlabeled anti-OX40 or anti-OX40L mAb, respectively. Streptavidin-allophycocyanin (BD Biosciences) was used in the second step of the staining. All of the samples were analyzed on a FACSCalibur flow cytometer (BD Immunocytometry Systems). The analyses were conducted using the CellQuest program (BD Immunocytometry Systems).

In vitro cell stimulation and recovery

A single-cell suspension was prepared from mouse spleens and incubated with mouse CD4 MicroBeads (Miltenyi Biotec) for 20 min at 4°C. The suspension was then purified by autoMACS. The purified CD4$^+$ T cells (purity >98%) were stimulated with 25 ng/ml PMA plus 1 μg/ml ionomycin (Sigma-Aldrich) or 10 μg/ml soluble anti-CD3 in the presence of irradiated (30 Gy) splenocytes, which were used as APCs, at 37°C for the indicated times. In some experiments, CD4$^+$ T cells were stimulated with plate-bound anti-CD3 (5 μg/ml) in the absence of APCs. In the case of OT-II T cell stimulation, irradiated (3000 rad) splenocytes that were pulsed with various concentrations of OVA peptide (323–339) were used as the APCs. Proliferation was measured in triplicate by the incorporation of [^{3}H]thymidine (1 μCi/well; Valeant Pharmaceuticals) during the last 8 or 12 h of each culture. In other proliferation studies, purified CD4$^+$ T cells were labeled with CFSE (Molecular Probes) by incubation with 2.5 μM CFSE in protein-free PBS for 10 min at 37°C; they were then diluted with a 10-fold volume of RPMI 1640 medium containing 10% FCS and incubated for 1 min. Cells were then washed twice with chilled PBS. The amount of cell division of CFSE-labeled cells was estimated by the reduction in fluorescence intensity, measured with a flow cytometer.

In vitro long-term T cell culture

Purified CD4$^+$ T cells from OT-II and OX40-KO OT-II mice were stimulated with the OVA peptide in the presence of irradiated (30 Gy) OX40L-KO splenocytes (APCs) in six-well plates. Every five days, one-half of the culture medium was exchanged. At the indicated time, cells were harvested and subjected to cell count, FACS analysis, and real-time PCR analysis for *OX40* and *OX40L* transcript. In vitro T cell survival was determined by trypan blue exclusion, and the calculation for percentage of survival was based on the input number of cells.

Coculture and Transwell experiments

CD4$^+$ T cells from OT-II OX40-KO mice were stimulated with OVA peptide in the presence of irradiated (3000 rad) OX40L-KO splenocytes (APCs) for 48 h. BW5147 cells, a mouse thymoma cell line, or the BW-mOX40 cells were added directly to the cell culture. Alternatively, to inhibit cell-cell contact, BW5147 or BW-mOX40 cells were placed in a 0.2-μm Anopore Membrane Nunc Tissue Culture Insert (Nalge Nunc International) and cultured in the presence of OX40L-expressing OT-II T cells. Twenty-four hours after the beginning of the coculture, OX40L expression on Vα2$^+$Vβ5.1-2$^+$ cells was examined with a flow cytometer. To inhibit receptor-mediated ligand internalization, 10 mM NaN_3 was added into the coculture. OX40-expressing primary T cells were also used instead of cell lines. To prepare OX40-expressing primary T cells, Ly-5.2$^+$ OX40L-KO OT-II T CD4$^+$ cells were stimulated with OVA peptide in the presence of irradiated (3000 rad) OX40L-KO splenocytes (APCs) for 48 h. Activated Ly-5.1$^+$ OX40-KO OT-II CD4$^+$ T cells and Ly-5.2$^+$ OX40L-KO OT-II T CD4$^+$, which can express OX40L and OX40, respectively, were cocultured in medium alone for 24 h. OX40L expression on Ly-5.1$^+$Vα2$^+$ cells was estimated by flow cytometry. To separate OX40L-expressing activated OX40-KO OT-II cells from OX40-expressing activated OX40L-KO OT-II cells, the latter cells were placed into a 0.2-μm Anopore Membrane Nunc Tissue Culture Insert.

Adoptive transfer experiments

Purified naive CD4$^+$ T cells (2.5–10 $\times$ 10^6) from the spleen and lymph nodes of OT-II or OT-II OX40L KO mice were injected i.v. into the tail vein of untreated or sublethally irradiated (500 cGy, ^{137}Cs source) congenic wild-type or OX40L-deficient recipient mice. In some cases, purified CD4$^+$ T cells were labeled with CFSE and then transferred to recipient mice. One day later, the mice were immunized with 2 mg of OVA protein (Worthington Biochemical) plus 50 μg of LPS (Sigma-Aldrich) or 50 μg of $OVA_{323-339}$ emulsified in CFA. The mice were sacrificed at the indicated times. To examine the endogenous expression of OX40L transcripts in vivo, OT-II T cells (1 $\times$ 10^7) were adoptively transferred into congenic wild-type recipient mice. One day later, the recipient mice were immunized, as described above. After the indicated time points, activated donor T cells were isolated magnetically from the spleen and peripheral lymph nodes of recipient mice using biotinylated anti-Ly-5.2 mAb, followed by anti-biotin MicroBeads (Miltenyi Biotec), and analyzed for OX40L expression. To show ex vivo expression of OX40L on T cells, OT-II and OT-II OX40-KO T cells (5 $\times$ 10^6) were adoptively transferred into congenic wild-type and OX40-deficient recipient mice, which then were immunized the next day, as described above. After the indicated time point, surface expression of OX40 and OX40L was examined on activated donor T cells.

Quantitative real-time PCR

A single-cell suspension of purified CD4$^+$ T cells was prepared and stimulated, as described above. At different time points, T cells were collected from the culture, and their total RNA was isolated using TRIzol reagent (Invitrogen Life Technologies). In a T cell transfer experiment, activated donor T cells were purified from recipient mice using a congenic marker (Ly-5). Total RNA was extracted from the purified donor T cells using TRIzol reagent. Single-strand cDNA was prepared by reverse transcribing 5 μg of total RNA using the SuperScript III kit (Invitrogen Life Technologies). Quantitative real-time PCR was conducted using TaqMan gene expression assays (Applied Biosystems; *OX40*; Mm00442039, *OX40L*; Mm00437214, *β-actin*; Mm00607939), according to the manufacturer's instructions. PCR thermal cycling conditions were 50°C for 2 min, 95°C for 10 min, and 40 cycles of 95°C for 15 s and 60°C for 1 min in a total volume of 25 μl/reaction. Data were collected using an 7500 Real Time PCR System and 7500 System Software (Applied Biosystems). All samples were run in triplicate, and the mean values were used for quantification. The expression level of each gene was normalized to the copies of *β-actin* mRNA from the same sample. Standard curves for *OX40* and *OX40L* were generated using seven serial dilutions (1/10, 1/10^2, 1/10^3, 1/10^4, 1/10^5, 1/10^6, and 1/10^7) of cDNA from stimulated CD4 T cells and cDNA from whole splenocyte of *OX40L* transgenic mice, respectively (linear regression R > 0.99). Standard curves for *β-actin* were created from same cDNA.

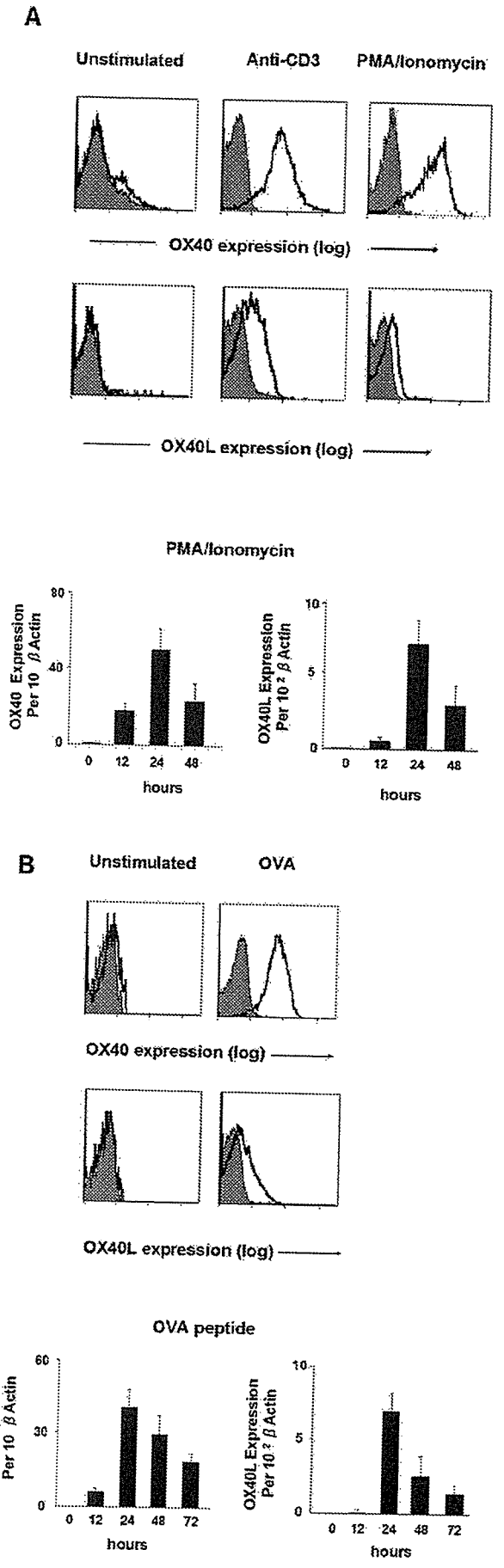

Results

Induction of endogenous OX40L expression by T cells upon Ag stimulation

To address whether the expression of OX40L on activated T cells is endogenous or derived from APCs, wild-type T cells were stimulated with PMA/ionomycin or anti-CD3. In a parallel experiment, OT-II $CD4^+$ T cells were stimulated with the OVA peptide in the presence of OX40L-deficient APCs, which excluded the potential for the T cells' acquisition of OX40L molecules from the APCs. Three days after stimulation, the up-regulation of OX40L expression as well as of OX40 expression was observed, implying that the OX40L expressed on the activated T cells was not derived from the APCs (Fig. 1, *A* and *B*, *upper panels*). We next analyzed the endogenous expression of the *OX40L* transcript by RT-PCR. Significant induction of *OX40* and *OX40L* transcripts was observed 24 h after stimulation, and the expression of both molecules was down-regulated after 72 h (Fig. 1, *A* and *B*, *lower panels*). The induction of *OX40L* gene expression in activated wild-type and OT-II T cells also confirmed that the *OX40L* that was up-regulated upon activation is endogenous.

Down-regulation of surface OX40L expression by OX40 through cell-cell contact

Pippig et al. (16) observed a higher surface expression of OX40L on activated OX40-KO T cells than on wild-type T cells. We found a similar increase in the expression of the OX40L protein on activated OX40-KO T cells (Fig. 2*A*). Upon evaluating the transcription levels of the *OX40L* gene, however, we found no significant difference between the OX40-KO and wild-type T cells (Fig. 2*B*). These results suggest that the surface expression of OX40L on T cells may normally be down-regulated by OX40 via a posttranscriptional mechanism. To determine whether the presence of OX40 can suppress the expression of OX40L on adjacent cells, OX40L-expressing CD4 T cells (OX40-KO OT-II cells previously stimulated with OVA) were cocultured with either an OX40-expressing T cell line (BW-mOX40) or the control parental cell line (BW5147) (Fig. 2*C*), and the surface expression of OX40L on the OX40-KO OT-II cells was monitored. Coculture with the BW-mOX40 cells markedly reduced the OX40L expression on activated OX40-KO OT-II cells, and the BW5147 parental cell lines did not affect the surface expression of OX40L on the OX40-KO OT-II cells (Fig. 2*C*). The reduced OX40L expression was not inhibited by azide treatment, which can inhibit

FIGURE 1. Expression of OX40 and OX40L on activated CD4 T cells. *A* and *B*, *upper panels*, Purified $CD4^+$ T cells (5×10^4) from wild-type mice were cultured in medium alone, and stimulated with either anti-CD3 (10 μg/ml) or PMA/ionomycin in the presence of irradiated OX40L-KO splenocytes (APCs) (2×10^5). In a parallel study, purified $CD4^+$ T cells (5×10^4) from OT-II TCR transgenic mice were cultured in medium alone or stimulated with OVA peptide (0.1 μM) in the presence of OX40L-KO APCs. Three days after stimulation, the OX40 and OX40L expression on $CD4^+$ cells was examined by flow cytometry (in the case of OT-II T cells, the gated $CD4^+V\alpha2^+$ T cells are shown). Filled histograms represent control staining. *A* and *B*, *lower panels*, Kinetics of *OX40* and *OX40L* mRNA expression. Total RNA was extracted from purified wild-type (*A*) or OT-II (*B*) T cells, which had been stimulated with either PMA/ionomycin or OVA peptide at the indicated times. The relative *OX40* and *OX40L* expression was quantified using real-time PCR, and the *OX40* and *OX40L* transcripts were normalized to the copies of *β-actin* mRNA from the same sample. The relative expression is expressed as the mean (±SD) of triplicate PCRs. Similar results were obtained in several independent experiments.

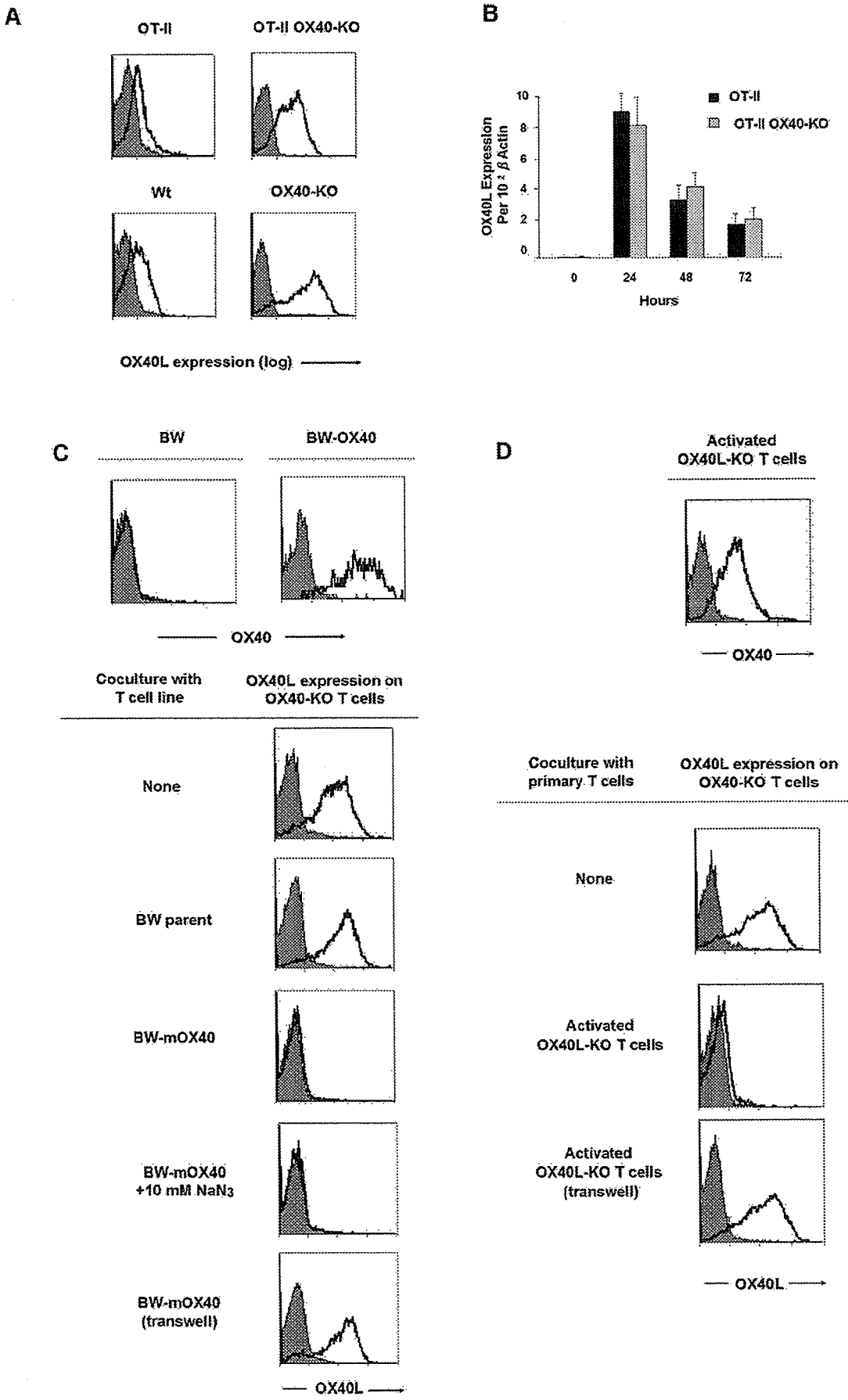
A
OT-II
OT-II OX40-KO
Wt
OX40-KO
OX40L expression (log)
B
OT-II
OT-II OX40-KO
OX40L Expression Per 10² β Actin
0
2
4
6
8
10
0
24
48
72
Hours
C
BW
BW-OX40
OX40
Coculture with T cell line
OX40L expression on OX40-KO T cells
None
BW parent
BW-mOX40
BW-mOX40 +10 mM NaN3
BW-mOX40 (transwell)
OX40L
D
Activated OX40L-KO T cells
OX40
Coculture with primary T cells
OX40L expression on OX40-KO T cells
None
Activated OX40L-KO T cells
Activated OX40L-KO T cells (transwell)
OX40L

ATP-dependent receptor internalization. Therefore, receptor internalization machinery may not be involved in the down-regulation of surface OX40L expression. Separating the OX40L-expressing T cells and OX40-expressing cells (BW-mOX40) with a Transwell culture system completely abrogated the reduction in OX40L expression, suggesting that cell-cell contact is required for the OX40 molecule to block OX40L expression (Fig. 2*C*). To further investigate whether OX40 expression by primary T cells could also suppress the OX40L expression on adjacent T cells, we cocultured Ly-5.1$^+$ OX40-KO OT-II T cells with Ly-5.2$^+$ OX40L-KO OT-II T cells. In this culture, OX40L was expressed by the OX40-KO T cells only, and OX40 was expressed by the OX40L-KO T cells only. Twenty-four hours after beginning the coculture, the expression level of OX40L on the activated OX40-KO T cells was markedly reduced (Fig. 2*D*). Separation of the two T cell populations abolished the suppression of OX40L expression by the OX40-expressing T cells (Fig. 2*D*). Furthermore, the reduction in OX40L expression in the presence of the OX40 receptor raises the possibility that the binding of OX40 to OX40L may reduce staining by the anti-OX40L mAb, which is inhibitory for the OX40-OX40L interaction. To address this question, we washed out cell surface of activated OT-II cells with an acid buffer (pH 3.0), which can abolish the binding between receptor and ligand (35), and then stained the cells with anti-OX40L mAb. However, the acid treatment did not increase the OX40L staining (data not shown). Collectively, these results provide clear evidence that the presence of the OX40 molecule can down-regulate OX40L expression through T cell-T cell contact after Ag stimulation.

Sustained OX40 and OX40L expression on long-lived T cells

Previous studies showed that, several days after Ag stimulation, CD4 T cells and activated APCs down-regulate the expression of OX40 and OX40L, respectively (6, 9, 39). To determine whether the expression levels of OX40 and OX40L were maintained on long-lived T cells, OT-II and OX40-KO OT-II T cells were stimulated with OVA in the presence of OX40L-deficient APCs, and the OX40 and OX40L expression levels on T cells were evaluated. For 14 days, OT-II T cells expressed significant amounts of *OX40* and *OX40L* mRNA (Fig. 3*A*). Although flow cytometric analysis showed quite low expression of OX40L on the OT-II T cells, OX40L expression on 30% of long-lived OT-II OX40-KO T cells was clearly seen (Fig. 3*B*). Because OT-II and OT-II OX40-KO T cells expressed comparable levels of *OX40L* transcripts (Fig. 3*A*, *lower panel*), the reduced surface OX40L expression on wild-type OT-II T cells may be due to the presence of the OX40 molecule. In addition, during the long-term culture, live OX40L-expressing cell number was also increased in OX40-deficient T cells (Fig. 3*C*). These data suggest that CD4 effector T cells can maintain the expression of both OX40 and OX40L after Ag priming.

OX40L expression on T cells contributes to T cell proliferation after antigenic stimulation

We next determined whether the expression of OX40L on T cells plays a functional role in immune responses. For this purpose, purified CD4$^+$ T cells from wild-type and OX40L-KO mice were stimulated with anti-CD3 in the presence of wild-type or OX40L-deficient APCs, and T cell proliferation was monitored. As shown in Fig. 4*A*, the absence of OX40L on either the T cells or APCs resulted in a significant reduction in T cell proliferation. Indeed, the presence of OX40L on both T cells and APCs is crucial for the optimal proliferation of CD4 T cells. Moreover, during the stimulation of CD4 T cells with plate-bound anti-CD3 (in the absence of APCs), the addition of an inhibitory anti-OX40L mAb suppressed the proliferation of wild-type T cells to the same level as OX40L-KO T cells (Fig. 4*B*). Because addition of anti-OX40L mAb (MGP34) to OX40-deficient T cells, which can express OX40L, showed no effect on T cell proliferation (Fig. 4*B*), cross-linking of OX40L on T cells cannot deliver any costimulatory or suppressive signals. Furthermore, the suppressive effect by the anti-OX40L mAb was abrogated by adding an agonistic anti-OX40 mAb (Fig. 4*C*), again suggesting that OX40 signals, but not OX40L signals, in T cells are responsible for CD4 T cell proliferation.

Previous reports demonstrated that in contrast to stimulation with anti-CD3, when TCR transgenic T cells are used, OX40 signals combined with Ag stimulation promote late cell division, rather than the induction of early cell proliferation (11, 40). Therefore, in addition to CD3 stimulation, we examined whether OX40L expression by T cells may also contribute to the late proliferation of OT-II T cells after Ag priming. OT-II OX40L-KO T cells that had received OX40 signals from OX40L-sufficient APCs proliferated similarly to OT-II T cells at day 3 of stimulation (Fig. 4*D*); however, they still showed less count of [^{3}H]TdR compared with OT-II T cells at the later phase as well as OT-II OX40-KO T cells (Fig. 4*D*). This implies

FIGURE 2. Suppression of OX40L surface expression on T cells in the presence of the OX40 receptor. *A*, Purified CD4$^+$ T cells (5×10^4) from wild-type or OX40-KO mice were stimulated with anti-CD3 (10 μg/ml) in the presence of irradiated OX40L-KO splenocytes (APCs) (2×10^5). Alternatively, purified CD4$^+$ T cells (5×10^4) from OT-II mice or OX40-KO OT-II mice were stimulated with OVA peptide (0.1 μM) in the presence of irradiated OX40L-KO splenocytes (APCs) (2×10^5). Filled histograms represent control staining. *B*, CD4$^+$ T cells from OT-II (■) and OT-II OX40-KO (▨) mice express similar levels of OX40L mRNA upon in vitro Ag stimulation. Total RNA was extracted from purified CD4$^+$ T cells, which had been stimulated with OVA peptide for the indicated time, and the relative OX40L expression was quantified, as described in Fig. 1*B*. The relative expression of OX40L transcript is expressed as the mean (±SD) of triplicate PCRs. Similar results were obtained in three independent experiments. *C* and *D*, The presence of OX40 suppresses OX40L expression through cell-to-cell contact. *C*, Purified OT-II OX40-KO CD4$^+$ T cells (5×10^4) were stimulated with OVA peptide in the presence of OX40L-deficient APCs for 48 h. OX40L-expressing T cells (OX40-KO OT-II, 5×10^4) were collected and cultured alone, in the presence of parental BW5147 (BW) cell line (5×10^3), with the BW5147 cells transfected with mouse OX40 (BW-mOX40) (5×10^3), for 24 h. OX40L expression on Vα2$^+$Vβ5.1-2$^+$ gated T cells was examined using flow cytometry. To block receptor-mediated ligand internalization, 10 mM azide was added into the coculture. To inhibit cell-cell contact, BW-mOX40- and OX40L-expressing T cells were cultured separately in a Transwell plate. Filled histograms represent control staining. Solid lines represent OX40 and OX40L expression on BW and OX40-KO T cells, respectively. *D*, OX40-KO Ly-5.1$^+$ OT-II T cells and OX40L-KO Ly-5.2$^+$ OT-II T cells were independently stimulated with OVA peptide in the presence of OX40L-deficient APCs for 48 h. OX40L-expressing cells (OX40-KO Ly-5.1$^+$ OT-II, 5×10^4) were collected and cultured either alone or in the presence of OX40-expressing cells (OX40L-KO Ly-5.2$^+$ OT-II, 5×10^4) for 24 h. OX40L expression on Ly-5.1$^+$Vα2$^+$ gated T cells was examined by flow cytometry. To inhibit cell-cell contact, OT-II OX40-KO Ly-5.1$^+$ and OT-II OX40L-KO Ly-5.2$^+$ were separated using a Transwell plate. Solid lines represent the OX40 and OX40L expression on activated OX40L-KO and OX40-KO T cells, respectively. Filled histograms represent control staining.

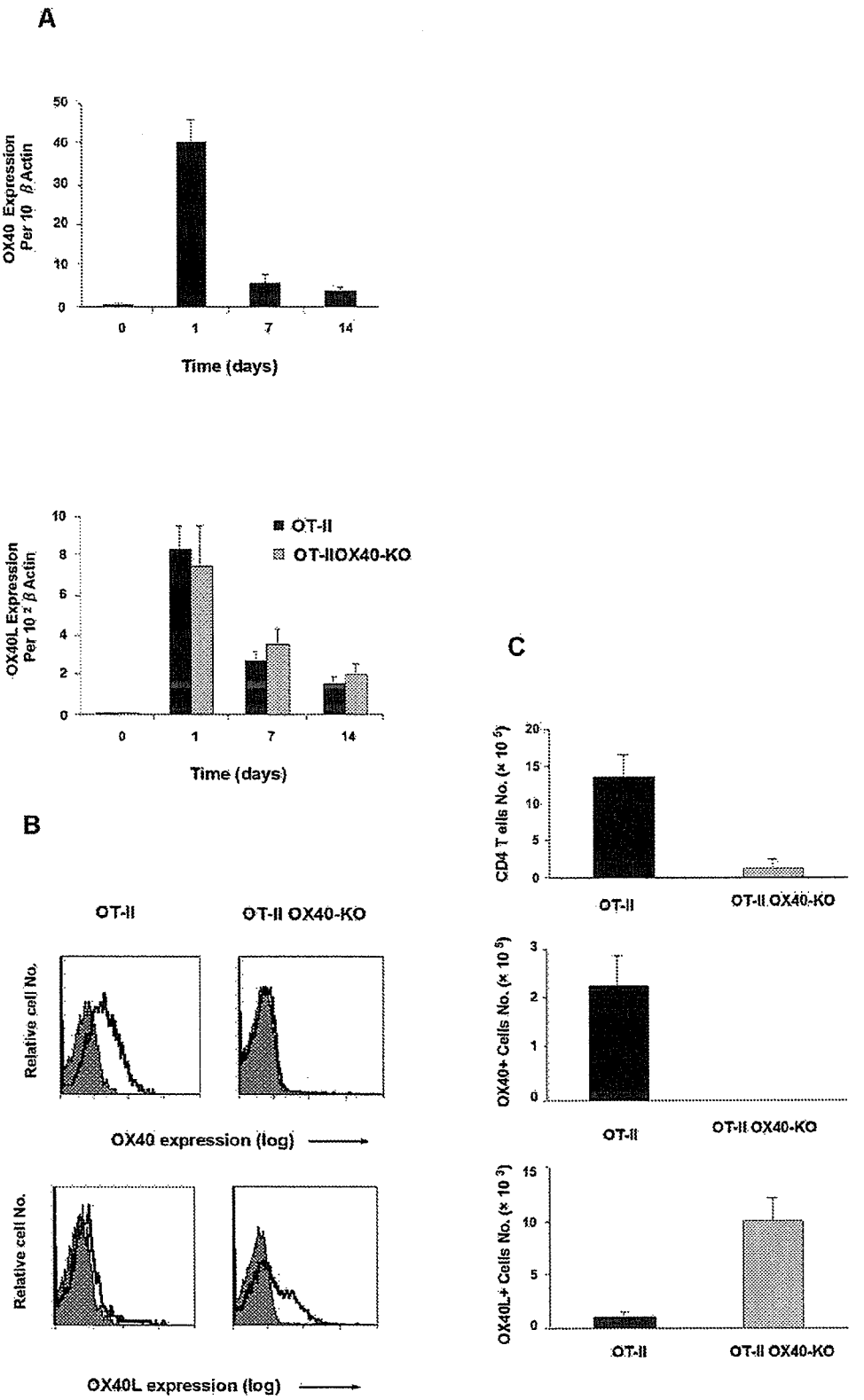

FIGURE 3. Sustained expression of *OX40* and *OX40L* by activated T cells. *A*, *upper panel*, Relative expression of the *OX40* transcript in activated OT-II cells. Purified $CD4^+$ T cells from OT-II mice were stimulated with the OVA peptide (0.1 μM) in the presence of irradiated OX40L-KO splenocytes (APCs) for the indicated time. Total RNA from the stimulated OT-II $CD4^+$ T cells was subjected to a quantitative real-time PCR for the *OX40* transcript, as described in Fig. 1*B*. The relative expression is expressed as the mean ($\pm$SD) of triplicate PCRs. *A*, *lower panel*, Relative expression of the *OX40L* transcript in activated OT-II (■) and OT-II OX40-KO T cells (▨). Purified $CD4^+$ T cells from OT-II or OX40-KO OT-II mice were stimulated with the OVA (0.1 μM) peptide in the presence of irradiated OX40L-KO splenocytes (APCs) for the indicated time, and total RNA from the stimulated T cells was subjected to a quantitative real-time PCR to amplify the *OX40L* transcript, as described in Fig. 1*B*. The relative expression is expressed as the mean ($\pm$SD) of triplicate PCRs. Similar results were obtained in three independent experiments. *B*, Purified $CD4^+$ T cells (2×10^6) from OT-II and OX40-KO OT-II mice were stimulated with the OVA peptide (0.1 μM) in the presence of irradiated OX40L-KO splenocytes (APCs) (1×10^7) in six-well plates. Fifteen days after the stimulation, OX40 and OX40L expression on $CD4^+V\alpha2^+$ T cells was examined. Solid lines represent the OX40 (*upper*) and OX40L (*lower*) expression on OT-II (*left*) or OX40-KO OT-II (*right*) T cells. Filled histograms represent control staining. *C*, Absolute number of total CD4 T cells (*upper*) and OX40 (*middle*)- and OX40L (*lower*)-expressing CD4 T cells, 15 days after Ag stimulation. In these figures, data are the average ($\pm$ SD) of triplicate cultures, and similar results were obtained in at least three independent experiments.

that OX40L on T cells contributes to late T cell proliferation or survival of T cells. Indeed, 5 days after stimulation in the presence of OX40L-deficient APCs (Fig. 4*E*), OT-II OX40-KO and OT-II OX40L-KO T cells showed a similar reduction in their proliferation, and this was most prominent when a low dose of OVA peptide was used. However, OT-II OX40L-KO T cells that received OX40 signals from OX40L-sufficient APCs proliferated more efficiently than OT-II OX40-KO T cells, but still showed impaired proliferation compared with wild-type T cells (Fig. 4*F*). Analysis of cell division using CFSE also showed slight impairment in cell proliferation of OT-II OX40-KO and OT-II OX40L-KO T cells (Fig. 4*G*). These results support the